

# Fingerprint matching of beyond-WIMP dark matter: neural network approach

Kyu Jung Bae<sup>a</sup>, Ryusuke Jinno<sup>a,b</sup>, Ayuki Kamada<sup>a</sup>, and Keisuke Yanagi<sup>c</sup>

<sup>a</sup> *Center for Theoretical Physics of the Universe, Institute for Basic Science (IBS), Daejeon 34126, Korea*

<sup>b</sup> *Deutsches Elektronen-Synchrotron DESY, 22607 Hamburg, Germany*

<sup>c</sup> *Department of Physics, University of Tokyo, Bunkyo-ku, Tokyo 113-0033, Japan*

## Abstract

Galactic-scale structure is of particular interest since it provides important clues to dark matter properties and its observation is improving. Weakly interacting massive particles (WIMPs) behave as cold dark matter on galactic scales, while beyond-WIMP candidates suppress galactic-scale structure formation. Suppression in the linear matter power spectrum has been conventionally characterized by a single parameter, the thermal warm dark matter mass. On the other hand, the shape of suppression depends on the underlying mechanism. It is necessary to introduce multiple parameters to cover a wide range of beyond-WIMP models. Once multiple parameters are introduced, it becomes harder to share results from one side to the other. In this work, we propose adopting neural network technique to facilitate the communication between the two sides. To demonstrate how to work out in a concrete manner, we consider a simplified model of light feebly interacting massive particles.

# Contents

<b>1</b>	<b>Introduction</b>	<b>1</b>
<b>2</b>	<b>Procedure for FIMP DM as an example</b>	<b>3</b>
2.1	Model $\rightarrow$ DM phase space distribution $\rightarrow$ Linear matter power spectrum . .	3
2.2	Linear matter power spectrum $\rightarrow$ Observables . . . . .	4
2.3	$\{\alpha, \beta, \gamma\}$ parametrization of the transfer function . . . . .	7
<b>3</b>	<b>Simplified FIMP model</b>	<b>8</b>
3.1	Freeze-in production . . . . .	8
3.2	Constraints . . . . .	10
<b>4</b>	<b>Neural network approach</b>	<b>10</b>
4.1	Neural network setup . . . . .	13
4.2	Model parameters $\rightarrow \{\alpha, \beta, \gamma\}$ . . . . .	14
4.3	$\{\alpha, \beta, \gamma\} \rightarrow$ Observables . . . . .	15
4.4	Combined results . . . . .	16
<b>5</b>	<b>Summary</b>	<b>16</b>
<b>A</b>	<b>Comparison with an analytic map</b>	<b>20</b>
<b>B</b>	<b>Further check: original data vs neural network</b>	<b>21</b>
<b>C</b>	<b>How to use the neural network data</b>	<b>23</b>

# 1 Introduction

Dark matter (DM) is an essential component for the Universe to form the current shape. Its existence and abundance are probed by gravitational observations such as galaxy rotation curves, bullet cluster collision, and cosmic microwave background (CMB) anisotropy. On the other hand, we have not seen any DM signal by any non-gravitational interactions, and thus we still do not know the identity of DM: what it is and how it is produced. One intriguing possibility is that DM consists of a new particle, which provides a clue to physics beyond the standard model (SM) (see Ref. [1] for a review).

One of the early attempts is a weakly interacting massive particle (WIMP) (see Refs. [2, 3] for recent reviews). In this direction, much efforts have been devoted at the large hadron collider (LHC) (for example, mono-jet searches [4, 5]) and at direct/indirect detection searches [6–9]. However, no firm signals have been reported yet. It may motivate us to consider beyond-WIMP scenarios that can be probed by cosmological/astrophysical observations.<sup>◇<sup>1</sup></sup> WIMPs behave as cold dark matter (CDM) on galactic scales. They are in good agreement with many independent observations such as CMB anisotropy [11] and galaxy clustering [12]. On the other hand, their predictions of galactic-scale structure are in debate. On galactic scales, there have been issues that are difficult to explain in CDM (small-scale issues).<sup>◇<sup>2</sup></sup> Alternatives to CDM may explain small-scale issues: warm dark matter (WDM) [15–17, 52, 56–60]; fuzzy DM [61–71]; and long-lasting DM interaction with primordial plasma or free-streaming light particles [60, 72–85].

On the other hand, impacts on galactic-scale structure formation depend on beyond-WIMP scenarios. Free-streaming of light WDM particles smears out the primordial density contrast. Quantum pressure of fuzzy DM prevents DM from gravitational clustering. Pressure of radiation to which DM couples involves DM in acoustic oscillation rather than gravitational clustering. Such effects are reflected in the linear matter power spectrum, which one can obtain by following evolution of the primordial density contrast. Generally by performing a suit of simulations with the resulting linear matter power spectrum, one can obtain observable quantities, which can be directly compared with cosmological/astrophysical observations. In summary, we need to work out the following procedure on a model-by-model basis:

Model  $\rightarrow$  Linear matter power spectrum  $\rightarrow$  Observables.

See the blue flow in Fig. 1. The whole procedure requires interdisciplinary expertise from particle phenomenology to (computational) astrophysics. Moreover, each step often requires a dedicated calculation. In particular, simulations in the last step are often too time-consuming to repeat.

---

<sup>◇<sup>1</sup></sup> We refer readers to Ref. [10] for a recent review of gravitational probes of DM properties.

<sup>◇<sup>2</sup></sup> Prominent examples are the missing satellite problem [13–17], core-cusp problem [18–21], and too-big-to-fail problem [22–27]. We refer readers to Ref. [28] for a recent review and further details. State-of-the-art hydrodynamical simulations have been demonstrating that astrophysical processes also play an important role [29–46]. There have also been reports that small-scale issues persist even in state-of-the-art hydrodynamical simulations [47–55]. To our best knowledge, it is still controversial if astrophysical processes fully resolve the small-scale issues.

One can work out each step independently by parametrizing the linear matter power spectrum. See the red flow in Fig. 1. A single parameter has been adopted conventionally: the thermal WDM mass  $m_{\text{WDM}}$ .<sup>◇<sup>3</sup></sup> On the other hand, a single parameter is not enough to cover a wide range of beyond-WIMP scenarios. For this purpose, Ref. [88] introduces the 3-parameter ( $\{\alpha, \beta, \gamma\}$ ) characterization of the linear matter power spectrum. On one side, one (likely particle physicist) can construct a map of model parameters onto  $\{\alpha, \beta, \gamma\}$ . On the other side, one (likely astrophysicist) can provide observational constraints on  $\{\alpha, \beta, \gamma\}$ , as indeed done for the Lyman- $\alpha$  forest data in Ref. [89]. By combining results from the two sides, one can obtain observational constraints on a given beyond-WIMP scenario. Nevertheless, once multiple parameters are introduced, it becomes hard to share results from one side to the other.

In this respect, we propose building ready-to-use networks: one maps model parameters onto  $\{\alpha, \beta, \gamma\}$ ; and another maps  $\{\alpha, \beta, \gamma\}$  onto observables. One can use these networks to examine models without repeating the aforementioned time-consuming procedure. Ideally, it would be the most efficient if one obtained analytic maps, but in reality, it is hard to establish such analytic maps. Thus, a numerical method is helpful to develop such effective maps. For this purpose, we adopt neural network technique.

To be concrete, in this paper, we consider a feebly interacting massive particle (FIMP) [90] (see Ref. [91] for a recent review). Light (keV-scale) FIMPs, which are produced through the freeze-in mechanism, are a compelling example of WDM. Even in FIMP models, the shape of suppression in the linear matter power spectrum depends on production processes such as 2-body decay, 3-body decay, and 2-to-2 scattering [92–98] (see Ref. [99] for a comprehensive discussion).<sup>◇<sup>4</sup></sup> Thus 3-parameter characterization rather than conventional single-parameter characterization is required to cover a wide range of FIMP models. By taking a simplified FIMP model, we demonstrate how one can work out the simplified procedure. We also provide the obtained neural networks through the arXiv website: one is a map of “model parameters  $\rightarrow \{\alpha, \beta, \gamma\}$ ” and the others are “ $\{\alpha, \beta, \gamma\} \rightarrow$  observables”.

The organization of this paper is following. In Sec. 2, we overview the conventional procedure to place constraints on FIMPs and describe the simplified procedure with the  $\{\alpha, \beta, \gamma\}$  parametrization. In Sec. 3, we introduce a simplified FIMP model. Our FIMP model shares many common aspects with a broad class of FIMP models. The basic production process is 2-body decay. We take into account late-time entropy production after freeze-in (case A) and also freeze-in production through 2-to-2 scattering (case B). In Sec. 4, we introduce neural network technique and work out the simplified procedure. We compare the constraints from the simplified procedure and those from the conventional procedure. Sec. 5 is devoted to the summary. In Appendix A, we compare our constraints to those obtained through an analytic map from the conventional thermal WDM mass. In Appendix B, we examine precision of

---

<sup>◇<sup>3</sup></sup> An underlying model may be light gravitino [86, 87]. WDM particles are thermalized in the early Universe and decouple from thermal plasma at some point.

<sup>◇<sup>4</sup></sup> We refer readers to Refs. [100–103] for sterile neutrino DM. Sterile neutrinos are produced through mixing with active neutrinos. We also refer readers to Ref. [104] for superWIMPs. SuperWIMPs are produced by the decay of WIMPs long after the WIMP freeze-out. If the WIMP decay occurs close after the WIMP freeze-out, one may need to take into account the momentum distribution function of WIMPs [105–109]. In this paper, we do not consider these possibilities, although they may be FIMPs in a broad sense.

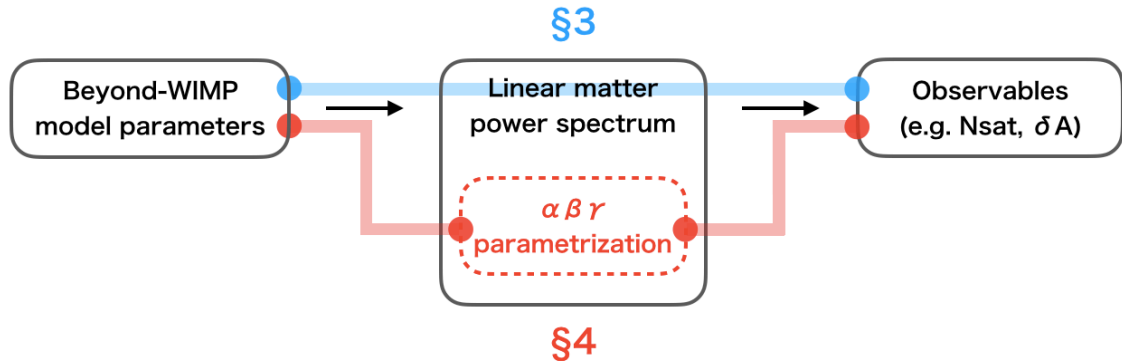


Figure 1: Sketch of the proposal of this paper.

the neural networks in detail. In Appendix C, we explain how to use the neural networks we provide.

## 2 Procedure for FIMP DM as an example

As we described in introduction, to study galactic-scale structure formation of beyond-WIMP scenarios, generically one has to take a 2-step procedure on a model-by-model basis:

$$\text{Model} \rightarrow \text{Linear matter power spectrum} \rightarrow \text{Observables}$$

(corresponding to the blue flow in Fig. 1). In the case of FIMP, the first step of “Model  $\rightarrow$  Linear matter power spectrum” actually consists of two steps:

$$\text{Model} \rightarrow \text{DM phase space distribution} \rightarrow \text{Linear matter power spectrum.}$$

To follow the two steps, one first needs to construct the collision term of the Boltzmann equation and integrate it to obtain the phase space distribution of the DM species. Then one has to follow evolution of the primordial density contrast with the obtained phase space distribution, possibly by using public cosmological Boltzmann solvers such as CLASS [110, 111]. In the following we overview this conventional procedure more specifically.

### 2.1 Model $\rightarrow$ DM phase space distribution $\rightarrow$ Linear matter power spectrum

We define the DM phase space distribution  $f_\chi(t, p)$  as a function of the cosmic time  $t$  and the physical momentum  $p$ , such that the DM number density is given by  $n_\chi = g_\chi \int d^3p / (2\pi)^3 f_\chi(t, p)$ , where  $g_\chi$  is the spin degrees of freedom. We assume that the DM phase space distribution  $f_\chi$  is much smaller than unity. We then obtain the phase space distribution at a late cosmic time  $t_f$  by integrating the collision term as

$$f_\chi(t_f, p) = \int_{t_i}^{t_f} dt \frac{1}{E_\chi} C \left( t, \frac{a(t_f)}{a(t_i)} p \right), \quad (2.1)$$

where  $t_i$  is the reheating time and  $a(t)$  is the cosmic scale factor. Given a squared matrix element of a specific production process, one obtains a semi-analytic expression of the corresponding collision term (see Ref. [99] for expressions).

FIMP production is most efficient when the heaviest particle in the process becomes non-relativistic (freeze-in mechanism). After that, FIMP particles free-stream and the phase space distribution is invariant as a function of the comoving momentum  $q \equiv p/T_\chi$ , where  $T_\chi$  is the effective DM temperature (see Sec. 3.1 for a specific expression of  $T_\chi$ ). Thus we use  $f(q) = f(t, p)$  to characterize the distribution. Practically, we fit the obtained phase space distribution of DM by

$$q^2 f(q) = \sum_{i=1}^N c_i q^{a_i} e^{-b_i q}, \quad (2.2)$$

where  $(a_i, b_i, c_i)$  are fitting parameters and  $i$  runs for different production processes.<sup>◇5</sup> We plug the fitting function into the public cosmological Boltzmann solver CLASS [110, 111] to obtain the linear matter power spectrum  $P(k)$  as a function of the wavenumber  $k$ . We use the cosmological parameters from “Planck 2015 TT, TE, EE+lowP” in Ref. [112]. Practically, we use the CLASS fluid approximation of non-cold DM.

## 2.2 Linear matter power spectrum $\rightarrow$ Observables

Galactic-scale structure places constraints on the linear matter power spectrum  $P(k)$ , or, the transfer function that is defined by

$$T^2(k) \equiv \frac{P(k)}{P_{\text{CDM}}(k)}. \quad (2.3)$$

It generically requires a suit of time-consuming simulations to obtain constraints on FIMP DM. We may simplify this step by using semi-analytic models and/or somehow converting the conventional thermal WDM mass  $m_{\text{WDM}}$ .

In the conventional thermal WDM model, WDM particles follow the Fermi-Dirac distribution with two spin degrees of freedom with temperature  $T_{\text{WDM}}$ . The relic abundance is expressed by  $m_{\text{WDM}}$  and  $T_{\text{WDM}}$  as

$$\Omega_{\text{WDM}} h^2 = \left( \frac{m_{\text{WDM}}}{94 \text{ eV}} \right) \left( \frac{T_{\text{WDM}}}{T_\nu} \right)^3 = 7.5 \left( \frac{m_{\text{WDM}}}{7 \text{ keV}} \right) \left( \frac{106.75}{g_*^{\text{WDM}}} \right). \quad (2.4)$$

For a given WDM mass, the temperature is determined such that the relic abundance reproduces the observed DM density. Note that for a keV-scale mass, somewhat large entropy production after decoupling is required for  $\Omega_{\text{WDM}} h^2 \simeq 0.12$ . On the other hand, FIMP DM has a different thermal history and thus different temperature and does not follow the

---

<sup>◇5</sup> One may wonder if we can work out “Model  $\rightarrow$  DM phase space distribution” and “DM phase space distribution  $\rightarrow$  Linear matter power spectrum” separately by using  $(a, b, c)$ . On one side, one can report constraints on  $(a, b, c)$ . On the other side, one can calculate  $(a, b, c)$  as a function of model parameters. It is worth investigating this possibility somewhere else.

Fermi-Dirac distribution. Thus reported lower bounds on  $m_{\text{WDM}}$  is not directly applicable to FIMP DM.

In this paper we consider the number of satellite galaxies [113–118] and Lyman- $\alpha$  forest [119–132] as observables.<sup>◇6</sup> Our analysis, which follows Refs. [88, 180], uses a semi-analytic model for the number of satellite galaxies and converts the reported lower bound on  $m_{\text{WDM}}$  for the Lyman- $\alpha$  forest.

## Number of satellite galaxies

One compares the predicted number of satellite galaxies  $N_{\text{sat}}$  in simulated Milky Way-size or M31-size haloes with the observed one. If the predicted number is smaller than the observed one, such FIMPs are excluded. This constraint may be conservative when one counts all the subhalos above a certain mass, since some of subhalos may not host galaxies bright enough to be detected.

We evaluate the number of satellite galaxies  $N_{\text{sat}}$  from the linear matter power spectrum in our FIMP model as follows. Ref. [118] develops a semi-analytic formula of the subhalo mass function in the conventional thermal WDM model. The formula uses the conditional mass function [181] based on the extended Press-Schechter approach [182] and the halo model (see Ref. [183] for a review). The formula adopts the top-hat filter function in the Fourier space (sharp- $k$  filter) to reproduce results of  $N$ -body simulations in the conventional thermal WDM model:

$$\frac{dN_{\text{sat}}}{d \ln M} = \frac{1}{C_n} \frac{1}{6\pi^2} \frac{M_0}{M} \frac{P(1/R)}{R^3 \sqrt{2\pi(S - S_0)}}, \quad (2.5)$$

where quantities with and without the subscript “0” denote those of the host halo and subhalo, respectively. For example,  $M$  ( $M_0$ ) is the subhalo (host halo) mass. The variance  $S$  is given by the linear matter power spectrum as

$$S = \frac{1}{2\pi^2} \int_0^{1/R} dk k^2 P(k). \quad (2.6)$$

The filter scale  $R$  is related with the mass as

$$M = \frac{4\pi}{3} \rho_m (cR)^3, \quad (2.7)$$

with the matter mass density at present  $\rho_m$ . Following Ref. [118], we adopt  $c = 2.5$  and  $C_n = 44.5$ . We use  $M_0 = 1.7 \times 10^{12} h^{-1} M_\odot$  as the Milky-Way mass, where  $h$  is the dimensionless Hubble constant. With these values, the number of satellite galaxies above  $M = 10^8 h^{-1} M_\odot$  is  $N_{\text{sat}} = 159$ , which is consistent with the result of the Aquarius simulation [184].  $M >$

---

<sup>◇6</sup> Other used probes include the delay of the reionization [133–139], the counts of high- $z$  gamma-ray bursts [140, 141], the faint end of luminosity function of high- $z$  galaxies [135, 136, 139, 142–146], the flux anomaly of quadrupole lens systems [147–154], and the redshifted 21 cm signal [155–162]. The counts of lensed distant supernovae [163] and direct collapse black holes [164] are suggested for a future use. We also refer readers to Ref. [165–179] for hydrodynamical simulation results differentiating WDM and CDM in galaxy formation.

$10^8 h^{-1} M_\odot$  roughly corresponds to the lower bound on the maximal circular velocity of  $V_{\max} > 10 \text{ km/s}$ .

We estimate the observed number of satellites above  $M = 10^8 h^{-1} M_\odot$  as  $N_{\text{sat}}^{\text{obs}} = 63$  (11 classical dwarf galaxies and  $3.5 \times 15$  ultra-faint dwarf galaxies).<sup>◇7</sup> We multiply 3.5 by the number of ultra-faint satellites found in SDSS to take account of the SDSS limited sky coverage as in Refs. [60, 88, 114–116, 118, 180].  $N_{\text{sat}} > N_{\text{sat}}^{\text{obs}}$  places a lower bound on the conventional thermal WDM mass as  $m_{\text{WDM}} > 2.9 \text{ keV}$ .<sup>◇8</sup> As we see,  $N_{\text{sat}}$  implicitly depends on the lower bound on the satellite mass. For example, once a number of smaller-size satellite galaxies are discovered in future, one has to repeat the above procedure by adjusting the lower bound on the satellite mass and scan model parameters on a model-by-model basis again. This drives us to use the  $\{\alpha, \beta, \gamma\}$  parametrization. Once the observational constraint on  $\{\alpha, \beta, \gamma\}$  is updated, one can easily update the constraint on models parameters by using a constructed map between model parameters and  $\{\alpha, \beta, \gamma\}$ .

## Lyman- $\alpha$ forest

Another observable is the Lyman- $\alpha$  forest in high-resolution quasar spectra. The flux power spectrum is a powerful probe of underlying galactic-scale structure, while the thermal history of the intergalactic medium has uncertainties. The most stringent constraint seems to exclude the WDM solution to small-scale issues [187].

The procedure for the Lyman- $\alpha$  forest constraint is an example of mapping the reported lower bound on the conventional thermal WDM mass onto a given model. We evaluate the impact of the WDM model on the Lyman- $\alpha$  forest data as follows. This approach follows Ref. [88], which extends the approach of Ref. [180]. First, given a 3-dimensional linear matter power spectrum  $P(k)$ , we calculate the 1-dimensional power spectrum as

$$P_{1\text{D}}(k) = \frac{1}{2\pi} \int_k^\infty dk' k' P(k'). \quad (2.8)$$

Second, we normalize the 1D power spectrum by that in the CDM model:

$$r(k) = \frac{P_{1\text{D}}(k)}{P_{1\text{D}}^{\text{CDM}}(k)}. \quad (2.9)$$

Third, we integrate  $r(k)$  over the typical range of  $k$  that a given Lyman- $\alpha$  forest spectrum probes:

$$A = \int_{k_{\min}}^{k_{\max}} dk r(k), \quad (2.10)$$

---

<sup>◇7</sup> Classical dwarfs: Sagittarius, LMC, SMC, Ursa Minor, Sculptor, Draco, Sextans, Carina, Fornax, LeoII, and LeoI. Ultra-faint dwarfs: Segue I, Ursa Major II, Segue II, Willman I, Coma Berenics, Bootes II, Bootes I, Pisces I, Ursa Major I, Hercules, Canes Venatici II, Leo IV, Leo V, Pisces II, Canes Venatici I. We refer readers to Refs. [185, 186] for dynamical properties. Note that  $V_{\max} \geq V_{1/2} \simeq \sqrt{3} \sigma_{\text{l.o.s}}$ , where  $V_{1/2}$  is the circular velocity at the half light radius and  $\sigma_{\text{l.o.s}}$  is the line-of-sight velocity dispersion [186].

<sup>◇8</sup> We remark that we do not use the fitting function given by Eq. (2.12), but directly compute the linear matter power spectrum by using CLASS [110, 111].



The dimensionless deviation of  $A$  represents net suppression in the Lyman- $\alpha$  forest spectrum:

$$\delta A = \frac{A_{\text{CDM}} - A}{A_{\text{CDM}}}. \quad (2.11)$$

Finally, we compare  $\delta A$  between our FIMP model and the conventional thermal WDM model with the reported lower bound on  $m_{\text{WDM}}$ . Note that one should use the typical range of  $k$  for  $A$  and the lower bound on  $m_{\text{WDM}}$  consistently from the same dataset or analysis. If  $\delta A > \delta A_{\text{WDM}}$ , then we regard our FIMP model is excluded.

Ref. [88] suggests  $k_{\text{min}} = 0.5 h/\text{Mpc}$  and  $k_{\text{max}} = 20 h/\text{Mpc}$  for the MIKE/HIRES+XQ-100 combined dataset used in Ref. [126]. The dataset places the lower bound of  $m_{\text{WDM}} > 3.5 \text{ keV}$  in the conventional thermal WDM model. We find that  $\delta A_{\text{WDM}} = 0.46$  for  $m_{\text{WDM}} = 3.5 \text{ keV}$ , <sup>◇<sup>9</sup></sup> so we use  $\delta A_{3.5 \text{ keV}} \equiv 0.46$  as an upper bound of  $\delta A$  of a given model. As we see,  $\delta A$  needs a data-dependent input  $k_{\text{min}}$  and  $k_{\text{max}}$  and thus one has to repeat the procedure for different dataset. A more extendable procedure is presumable. Our proposal is the  $\{\alpha, \beta, \gamma\}$  parameterization. For a given new dataset, while one has to update constraints in terms of in terms of  $\{\alpha, \beta, \gamma\}$ , one can use the constructed map between model parameters and  $\{\alpha, \beta, \gamma\}$  as it is.

### 2.3 $\{\alpha, \beta, \gamma\}$ parametrization of the transfer function

As we described above, the thermal WDM model has been conventionally used to report observation constraints on the transfer function  $T^2(k)$ . The single-parameter fitting function of  $T^2(k)$  in the thermal WDM model is given by [57, 119, 188] <sup>◇<sup>10</sup></sup>

$$T_{\text{WDM}}^2(k) = [1 + (\alpha k)^{2\nu}]^{-10/\nu}. \quad (2.12)$$

Here  $\nu = 1.12$  and thus only  $\alpha$  is a parameter related with the thermal WDM mass:

$$\alpha = 0.049 \text{ Mpc}/h \left( \frac{m_{\text{WDM}}}{\text{keV}} \right)^{-1.11} \left( \frac{\Omega_{\text{WDM}}}{0.25} \right)^{0.11} \left( \frac{h}{0.7} \right)^{1.22} \quad (2.13)$$

from Ref. [119].

However, the single-parameter ( $m_{\text{WDM}}$ ) characterization does not cover a wide range of beyond-WIMP models. Ref. [88] proposes characterizing the transfer function as

$$T^2(k) = [1 + (\alpha k)^\beta]^{2\gamma}. \quad (2.14)$$

This parametrization allow us to divide the procedure to place constraints on FIMPs into two with  $\{\alpha, \beta, \gamma\}$  being a ‘‘common language’’. On one side, one calculates  $\{\alpha, \beta, \gamma\}$  as a function of model parameters in a given model (corresponding to the left red flow in

---

<sup>◇<sup>9</sup></sup> We again remark that we do not use the fitting function given by Eq. (2.12), but directly compute the linear matter power spectrum by using CLASS [110, 111]. This may be partially why our  $\delta A_{\text{WDM}} = 0.46$  is different from  $\delta A_{\text{WDM}} = 0.38$  in Ref. [88].

<sup>◇<sup>10</sup></sup> We refer readers to Ref. [102] for a fitting function of  $T^2(k)$  in the resonantly produced sterile neutrino DM.

Fig. 1). On the other side, one reports a likelihood function from observations as a function of  $\{\alpha, \beta, \gamma\}$  (corresponding to the right red flow in Fig. 1). By combining these two, one can obtain the constraints on model parameters more easily. This procedure is also very extendable. Once a new observation date becomes available, what one has to do is just to update the latter, namely, constraints on  $\{\alpha, \beta, \gamma\}$ . One does not need to repeat the former. One can use a constructed map between model parameters and  $\{\alpha, \beta, \gamma\}$  as it is.

A remaining challenge is how to share results from the two sides. It is not apparent how to share 3-parameter results efficiently. In this paper, we propose using neural network technique. In the context of the paper, advantages of using a neural network are:

- It expresses nonlinear relations quite efficiently.
- It learns nonlinearity without being explicitly taught.
- It provides us with a unified format in presenting results.

We indeed see these advantages in Sec. 4.

### 3 Simplified FIMP model

In this work, we consider a simple setup. The model contains a seemingly renormalizable interaction of Majorana DM  $\chi$  with a heavy Dirac fermion  $\Psi$  and a heavy scalar  $\phi$ :

$$\mathcal{L}_\chi = y_\chi \phi \bar{\Psi} \chi + \text{h.c.}, \quad (3.1)$$

with the Yukawa coupling  $y_\chi$ . We assume the mass hierarchy of  $m_\Psi > m_\phi \gg m_\chi$ .<sup>◇11</sup>

This simplified model virtually corresponds to a light axino FIMP model considered in Refs. [99, 189]. The axino FIMP model is based on a supersymmetric version of Dine-Fischler-Srednicki-Zhitnitsky axion model [190, 191]. Axino is a fermionic supersymmetric partner of axion that dynamically explains why the strong interaction preserves  $CP$  very precisely [192–195]. One can identify  $\chi$ ,  $\Psi$ , and  $\phi$  as light axino, Higgsino (supersymmetric partner of Higgs), and Higgs in the axino FIMP model.

#### 3.1 Freeze-in production

We assume that  $\Psi$  is equilibrated in thermal plasma. Freeze-in production of DM  $\chi$  proceeds mainly through 2-body decay of  $\Psi \rightarrow \phi + \chi$ . The production process ceases (decouples) when the plasma temperature  $T$  gets comparable with the mother particle mass; *i.e.*, the decoupling temperature is  $T_{\text{dec}} \sim m_\Psi$ .

It is convenient to define a DM “temperature” as

$$T_{\text{DM}} = \left( \frac{g_*(T)}{g_*(T_{\text{dec}})} \right)^{1/3} T, \quad (3.2)$$

<sup>◇11</sup> The result will change only slightly for  $m_\phi > m_\Psi \gg m_\chi$  and for different quantum statistics of particles [99].

with the effective number of massless degrees of freedom  $g_*(T)$  and the decoupling temperature  $T_{\text{dec}}$ . This temperature scales as  $T_{\text{DM}} \propto 1/a$  with the cosmic scale factor  $a(t)$  and thus the dimensionless momentum  $q = p/T_{\text{DM}}$  is conserved after the decoupling. In the following, we take  $g_*(T_{\text{dec}}) = g_*^{\text{SM}} = 106.75$  (all the SM particles) as a baseline value.

### Case A: Decay with entropy production

Meanwhile, we incorporate a different value of  $g_*(T_{\text{dec}})$  or entropy production after the decoupling, by introducing  $\Delta$  as

$$T_{\text{DM}} = \left( \frac{g_*(T)}{\Delta \times g_*^{\text{SM}}} \right)^{1/3} T. \quad (3.3)$$

$\Delta > 1$  takes account of entropy production after the decoupling, or larger degrees of freedom at the decoupling (*e.g.*, minimal supersymmetric standard model, where  $g_*^{\text{MSSM}} = 226.75$ ).  $\Delta < 1$  is applied to the case of late decoupling, *i.e.*,  $g_*(T_{\text{dec}}) < g_*^{\text{SM}}$ .

We take into account only relevant model parameters to “warmness” of FIMP DM. Note that warmness of FIMP DM depends on the phase space distribution  $f(p)$  (equivalently,  $f(q)$  and  $T_{\text{DM}}$ ) and the FIMP mass  $m_\chi$ . The phase space distribution does not depend on an absolute scale of  $m_\phi$  and  $m_\Psi$ , but is *sensitive* to the ratio  $m_\phi/m_\Psi$  since the ratio determines the kinematic phase space of decay product, *i.e.*,  $\chi$  in this case. If the two masses are degenerate, the energy of  $\chi$  in  $\Psi \rightarrow \phi + \chi$  is suppressed and thus the resultant  $\chi$ 's are colder [98, 99, 189].

In this class of models, therefore, the relevant parameters are

$$\frac{m_2}{m_1}, \quad m_{\text{DM}}, \quad \Delta. \quad (3.4)$$

Hereafter we use the notation of  $m_1 = m_\Psi$ ,  $m_2 = m_\phi$ , and  $m_{\text{DM}} = m_\chi$  for the sake of notational simplicity. The Yukawa coupling  $y_\chi$  is fixed by the observed DM abundance  $\Omega_{\text{DM}} = m_\chi s_0 Y_\chi / \rho_c$ . While the colder phase space distribution is realized for a more degenerate mass spectrum, the larger Yukawa coupling or lighter  $\Psi$  is necessary to obtain the observed DM abundance.

### Case B: Decay with scattering

Generally a daughter particle  $\phi$  has another interaction with a light Dirac fermion  $f$ :

$$\mathcal{L}_\phi = y_f \phi \bar{f} f + \text{h.c.}, \quad (3.5)$$

with the Yukawa coupling  $y_f$ . One can identify  $f$  as top quark (again  $\phi$  as Higgs) in the axino FIMP model [99, 189]. We assume the mass hierarchy of  $m_\Psi > m_\phi \gg m_f$ . We also assume that  $f$  is equilibrated in thermal plasma. In this case, freeze-in production of  $\chi$  occurs through  $s$ -channel scattering of  $f\bar{f} \rightarrow \Psi\chi$  and  $t$ -channel scattering of  $\Psi f \rightarrow \chi f$  as well as through 2-body decay of  $\Psi \rightarrow \phi + \chi$ . The decoupling temperature is again  $T_{\text{dec}} \sim m_\Psi$ .  $y_f$  determines the scattering contribution to the yield,  $Y_{\text{scat}}$ . Freeze-in production through

scattering becomes more important for more degenerate  $\phi$  and  $\Psi$ , since the partial decay width becomes smaller.

In summary, in this case, the relevant parameters are

$$\frac{m_2}{m_1}, \quad \frac{Y_{\text{scat}}}{Y_{\text{total}}}, \quad m_{\text{DM}}. \quad (3.6)$$

Again hereafter we use the notation of  $m_1 = m_\Psi$ ,  $m_2 = m_\phi$ , and  $m_{\text{DM}} = m_\chi$  for the sake of notational simplicity.  $y_\chi$  is fixed by the observed DM abundance:  $Y_{\text{dec}} + Y_{\text{scat}} = Y_{\text{total}}$ . In this case, we do not vary  $\Delta$  but take several values such as  $\Delta = 0.3, 1$ , and  $3$ .

## 3.2 Constraints

We derive constraints from  $N_{\text{sat}}$  and from  $\delta A$  through the conventional procedure described in Sec. 2 (corresponding to the blue flow in Fig. 1).

First we present constraints from  $N_{\text{sat}}$  in Fig. 2. The top-left panel is for Case A (Decay with entropy production), while the other panels are for Case B (Decay with scattering). For Case A, bluer regions satisfy the condition  $N_{\text{sat}} > N_{\text{sat}}^{\text{obs}} = 63$  for each value of  $\Delta$ . For Case B, the three panels correspond to  $\Delta = 0.3$  (top-right),  $\Delta = 1$  (bottom-left), and  $\Delta = 3$  (bottom-right), respectively. As in Case A, bluer regions satisfy  $N_{\text{sat}} > N_{\text{sat}}^{\text{obs}}$  for each value of  $m_{\text{DM}}$ . We also display two lines corresponding to  $y_f = \sqrt{\pi/3}$  (red-dashed) and  $y_f = \sqrt{1/3}$  (red-dotted), to depict a perturbative Unitarity limit.

Next we show constraints from  $\delta A$  in Fig. 3. The four panels are for Case A (top-left) and for Case B with  $\Delta = 0.3$  (top-right),  $\Delta = 1$  (bottom-left), and  $\Delta = 3$  (bottom-right), respectively. For each parameter, bluer regions satisfy the condition  $\delta A < \delta A_{3.5 \text{ keV}}$ . The red lines are the same as Fig. 2. We see that  $\delta A$  gives stronger constraints than  $N_{\text{sat}}$ .

As repeatedly stated, constraints on the transfer function are often provided in terms of the conventional thermal WDM mass  $m_{\text{WDM}}$ . In Appendix A we convert  $m_{\text{WDM}} > 2.9 \text{ keV}$  corresponding to  $N_{\text{sat}} > N_{\text{sat}}^{\text{obs}}$  and  $m_{\text{WDM}} > 3.5 \text{ keV}$  corresponding to  $\delta A < \delta A_{3.5 \text{ keV}}$  into constraints on our FIMP parameters. We see that the constraints are qualitatively similar but quantitatively slightly different ( $\sim 10\%$  in  $m_{\text{DM}}$ ) from those derived in this section.

## 4 Neural network approach

As stressed in Sec. 1, one of the main purposes of this paper is to provide ready-to-use maps for “Model parameters  $\rightarrow \{\alpha, \beta, \gamma\}$ ” and also for “ $\{\alpha, \beta, \gamma\} \rightarrow$  Observables” (see the red flow in Fig. 1). Our proposal is to use a neural network for this purpose. In the following we first explain our neural network setup in Sec. 4.1, and then construct concrete neural networks for “Model parameters  $\rightarrow \{\alpha, \beta, \gamma\}$ ” and “ $\{\alpha, \beta, \gamma\} \rightarrow$  Observables” in Sec. 4.2 and Sec. 4.3, respectively. Finally we combine the two neural networks to reproduce the constraints presented in Sec. 3 to demonstrate the precision of the neural networks.

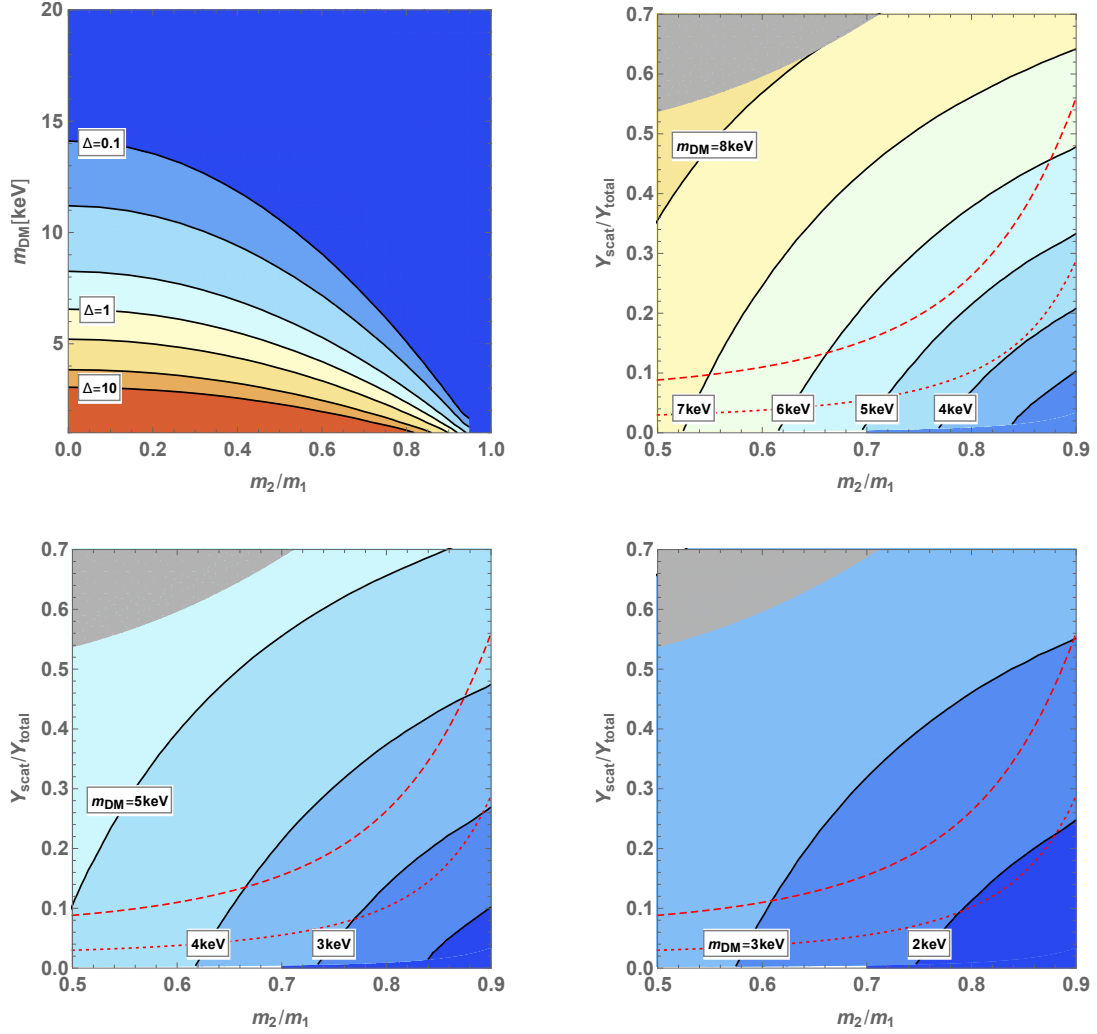


Figure 2: Constraints from  $N_{\text{sat}} > N_{\text{sat}}^{\text{obs}}$ , where  $N_{\text{sat}}^{\text{obs}} = 63$  is the observed value explained in the main text. Bluer regions are alive for each value of  $m_{\text{DM}}$ . The red contours are for  $y_f = \sqrt{\pi/3}$  (dashed) and  $\sqrt{1/3}$  (dotted). **Top-left:** Case A (Decay with entropy production). **Top-right:** Case B (Decay with scattering) with  $\Delta = 0.3$ . **Bottom-left:** Case B with  $\Delta = 1$ . **Bottom-right:** Case B with  $\Delta = 3$ .

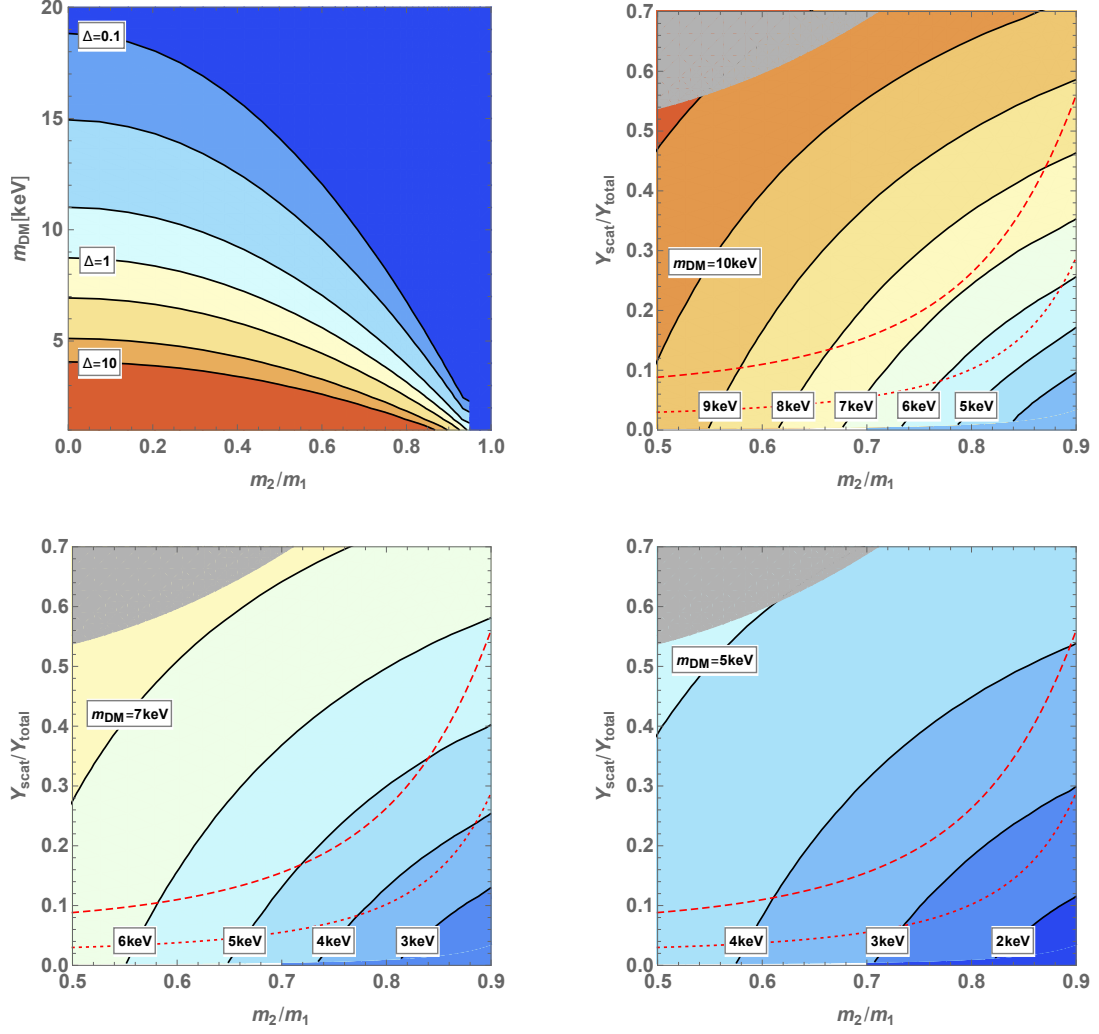


Figure 3: Constraints from  $\delta A > \delta A_{3.5 \text{ keV}}$ , where  $\delta A_{3.5 \text{ keV}} = 0.46$  is the value for 3.5 keV thermal WDM. Bluer regions are alive for each contour. **Top-left:** Case A (Decay with entropy production). **Top-right:** Case B (Decay with scattering) with  $\Delta = 0.3$ . **Bottom-left:** Case B with  $\Delta = 1$ . **Bottom-right:** Case B with  $\Delta = 3$ .

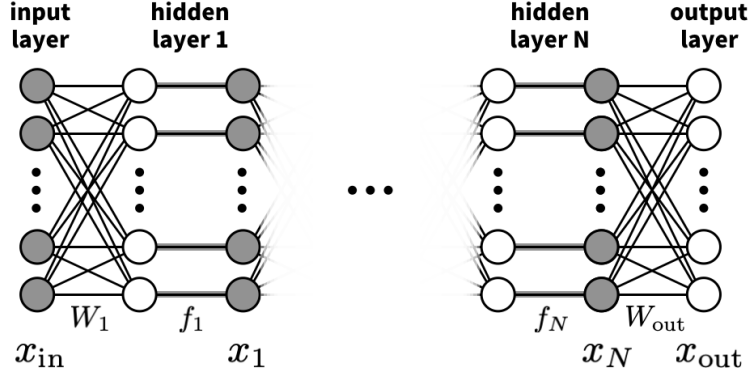


Figure 4: Schematic diagram of the neural network. Partly taken from Ref. [196].

## 4.1 Neural network setup

The setup of our neural network is summarized in Fig. 4. We identify the input vector  $\vec{x}_{\text{in}}$  as the three model parameters for each of Case A and B. As the layer proceeds, the original layer is operated by linear algebra and then multiplied by a nonlinear function  $\vec{f}$ . More concretely, the connections among the layers are given by

$$\vec{x}_1 = \vec{f}(W_1 \vec{x}_{\text{in}} + \vec{b}_1), \quad (4.1)$$

$$\vec{x}_n = \vec{f}(W_n \vec{x}_{n-1} + \vec{b}_n) \quad (2 \leq n \leq N), \quad (4.2)$$

$$\vec{x}_{\text{out}} = W_{\text{out}} \vec{x}_N + \vec{b}_{\text{out}}, \quad (4.3)$$

where  $N$  is the number of hidden layers and  $W$ 's and  $b$ 's are called weight matrices and biases, respectively. The nonlinear function  $\vec{f}$  is understood as acting on each component:

$$\vec{f}(\vec{y}) \equiv \begin{pmatrix} f(y_1) \\ f(y_2) \\ \vdots \end{pmatrix}, \quad (4.4)$$

and we adopt a Rectified Linear Unit (ReLU) [197] for the  $f$  function:

$$f(y) = \max(0, y). \quad (4.5)$$

We train the neural network with supervised learning. As we explain in the next subsections, we collect  $\mathcal{O}(10,000)$  combinations of the input  $\vec{x}_{\text{in}}$  and the true value (from direct calculations) of the output  $\vec{x}_{\text{out}}^{(\text{true})}$ . Note that, with such a large number of data points, it is much more efficient to recast the obtained data onto the neural network and share the neural network parameters than to provide the data itself. Training of the neural network is performed through the updates of the weight matrices and biases so that the output of the neural network  $\vec{x}_{\text{out}}$  gets closer to the true value  $\vec{x}_{\text{out}}^{(\text{true})}$ . The closeness is measured by the loss function  $E$ , which we take as

$$E = \sum_i \left| \left( \vec{x}_{\text{out}}^{(\text{true})} \right)_i - \left( \vec{x}_{\text{out}} \right)_i \right|, \quad (4.6)$$

where  $(\vec{x})_i$  denotes the  $i$ -th component of  $\vec{x}$ .

For the number of hidden layers, we use  $N = 2$  in this paper. Then the relation between the input and output reduces to

$$\vec{x}_{\text{out}} = W_{\text{out}} \vec{f} \left( W_2 \vec{f} \left( W_1 \vec{x}_{\text{in}} + \vec{b}_1 \right) + \vec{b}_2 \right) + \vec{b}_{\text{out}}. \quad (4.7)$$

We construct the neural network using the public code `TensorFlow` [198],<sup>◇12</sup> and train it for  $\mathcal{O}(10^5)$  epochs. The whole dataset is split into training (90%) and test (10%) subsets, and the former is used to train the neural network, while the latter is used to monitor the training process and avoid possible overfitting. We also apply a 10% dropout [199] to avoid overfitting. We use Adam Optimizer [200] with a learning rate of 0.001.

## 4.2 Model parameters $\rightarrow \{\alpha, \beta, \gamma\}$

We first construct a neural network connecting model parameters and the transfer function parameters  $\{\alpha, \beta, \gamma\}$ . Before moving on, however, we remark that parameter degeneracy often appears when we fit  $\{\alpha, \beta, \gamma\}$  to the resulting power spectrum in the simplified FIMP model in Sec. 3. Indeed Ref. [88] also notices this parameter degeneracy (see Appendix. A of Ref. [88]). Meanwhile, Ref. [89] reports that the combination of  $|\beta \times \gamma|$  is well constrained by observational data (see Fig. 4 of Ref. [89]), while the orthogonal direction  $\beta/\gamma$  is not very sensitive. Therefore, in this paper, we fix this orthogonal direction by the relation

$$\gamma = -\beta. \quad (4.8)$$

As a result, the output  $\vec{x}_{\text{out}}$  becomes a two-component vector.

### Case A: Decay with entropy production

Let us first take Case A (see Sec. 3.1). We identify the output  $\vec{x}_{\text{out}}$  and input  $\vec{x}_{\text{in}}$  as

$$\vec{x}_{\text{in}} = \begin{pmatrix} \frac{\log_{10} \left( 1 - \frac{m_2}{m_1} \right) - (\vec{x}_{\text{in},0})_1}{(\vec{\sigma}_{\text{in}})_1} \\ \frac{\log_{10} m_{\text{DM}} [\text{keV}] - (\vec{x}_{\text{in},0})_2}{(\vec{\sigma}_{\text{in}})_2} \\ \frac{\log_{10} \Delta - (\vec{x}_{\text{in},0})_3}{(\vec{\sigma}_{\text{in}})_3} \end{pmatrix}, \quad \vec{x}_{\text{out}} = \begin{pmatrix} \frac{\log_{10} \alpha - (\vec{x}_{\text{out},0})_1}{(\vec{\sigma}_{\text{out}})_1} \\ \frac{\log_{10} \beta - (\vec{x}_{\text{out},0})_2}{(\vec{\sigma}_{\text{out}})_2} \end{pmatrix}. \quad (4.9)$$

Here  $\vec{x}_{\text{in},0}$  and  $\vec{x}_{\text{out},0}$  are the means of the input and output data, respectively, while  $\vec{\sigma}_{\text{in}}$  and  $\vec{\sigma}_{\text{out}}$  are the standard deviations. These are constant vectors introduced to normalize the data and make learning more efficient.

For the dataset, we sample about 20,000 data points from  $0 < m_2/m_1 < 1$ ,  $1 \leq m_{\text{DM}} [\text{keV}] \leq 20$ , and  $0.1 \leq \Delta \leq 10$ . We exclude data points in the gray-shaded regions of

<sup>◇12</sup> We use the version `r1.1.7`.



Figs. 5 and 6, and thus the resulting neural networks cannot be used for the input parameters in these regions. <sup>◇13</sup>

### Case B: Decay with scattering

Next let us take Case B (see Sec. 3.1). We identify the output  $\vec{x}_{\text{out}}$  and input  $\vec{x}_{\text{in}}$  as

$$\vec{x}_{\text{in}} = \begin{pmatrix} \frac{\log_{10} \left( 1 - \frac{m_2}{m_1} \right) - (\vec{x}_{\text{in},0})_1}{(\vec{\sigma}_{\text{in}})_1} \\ \frac{\log_{10} \frac{Y_{\text{scat}}}{Y_{\text{total}}} - (\vec{x}_{\text{in},0})_2}{(\vec{\sigma}_{\text{in}})_2} \\ \frac{\log_{10} m_{\text{DM}} - (\vec{x}_{\text{in},0})_3}{(\vec{\sigma}_{\text{in}})_3} \end{pmatrix}, \quad \vec{x}_{\text{out}} = \begin{pmatrix} \frac{\log_{10} \alpha - (\vec{x}_{\text{out},0})_1}{(\vec{\sigma}_{\text{out}})_1} \\ \frac{\log_{10} \beta - (\vec{x}_{\text{out},0})_2}{(\vec{\sigma}_{\text{out}})_2} \end{pmatrix}. \quad (4.10)$$

For the dataset, we sample about 20,000 data points from  $0.5 < m_2/m_1 < 0.9$ ,  $0 \leq Y_{\text{scat}}/Y_{\text{total}} \leq 0.7$ , and  $1 \leq m_{\text{DM}} [\text{keV}] \leq 15$ . We again exclude data points in the gray-shaded regions of Figs. 5 and 6.

### 4.3 $\{\alpha, \beta, \gamma\} \rightarrow \text{Observables}$

We next construct a neural network that maps  $\{\alpha, \beta, \gamma\}$  onto the observables, more specifically,  $N_{\text{sat}}$  and  $\delta A$  introduced in Sec. 2. We identify the input and output as

$$\vec{x}_{\text{in}} = \begin{pmatrix} \frac{\log_{10} \alpha - (\vec{x}_{\text{in},0})_1}{(\vec{\sigma}_{\text{in}})_1} \\ \frac{\log_{10} \beta - (\vec{x}_{\text{in},0})_2}{(\vec{\sigma}_{\text{in}})_2} \\ \frac{\log_{10}(-\gamma) - (\vec{x}_{\text{in},0})_3}{(\vec{\sigma}_{\text{in}})_3} \end{pmatrix}, \quad (4.11)$$

$$\vec{x}_{\text{out}} = \left( \frac{\log_{10} N_{\text{sat}} - (\vec{x}_{\text{out},0})_1}{(\vec{\sigma}_{\text{out}})_1} \right) \quad \text{or} \quad \left( \frac{\log_{10} \delta A - (\vec{x}_{\text{out},0})_1}{(\vec{\sigma}_{\text{out}})_1} \right). \quad (4.12)$$

Note that we do not assume  $\gamma = -\beta$  in contrast to the previous subsection, and thus  $\vec{x}_{\text{in}}$  is a three-component vector. This is to accommodate broader class of models than the models we adopt in this paper. Also note that  $\vec{x}_{\text{out}}$  is a one-component vector, which means that we construct neural networks for “ $\{\alpha, \beta, \gamma\} \rightarrow N_{\text{sat}}$ ” and for “ $\{\alpha, \beta, \gamma\} \rightarrow \delta A$ ” separately.

For the dataset, we sample about 70,000 points from  $0.001 \leq \alpha \leq 0.1$ ,  $0.1 \leq \beta \leq 10$ , and  $0.1 \leq \gamma \leq 10$ .

<sup>◇13</sup> The reason for excluding the gray-shaded regions is as follows. For Case A, the right-top corner of the parameter space corresponds to the CDM limit. Since the transfer function approaches unity in this region, the parameter set  $\{\alpha, \beta, \gamma\}$  are not uniquely determined by fitting even after  $\gamma = -\beta$  is imposed. For Case B, the left-top corner corresponds to the large Yukawa coupling limit and thus the perturbative Unitarity violation problem arises.

## 4.4 Combined results

Before combining the two neural networks constructed in the previous subsections, we remark that we discuss details about the precision of the neural network in Appendix B. We provide the resultant neural network parameters through the `arXiv` website. See Appendix C for further explanation of the data files. We also provide a `Mathematica` file (`freeze-in.nb`) for illustration.

Now let us check the precision of the neural network by combining the two neural networks. The results should coincide with the constraints obtained in Sec. 3 as long as the neural networks work well. Figs. 5 and 6 are the constraints from  $N_{\text{sat}} > N_{\text{sat}}^{\text{obs}}$  and  $\delta A < \delta A_{3.5\text{keV}}$  derived through the combination of the two neural networks and thus should be compared with Figs. 2 and 3, respectively. We see that the neural networks nicely reproduce the original constraints.

We again stress constructing nonlinear maps for “Model parameters  $\rightarrow$  Linear matter power spectrum” and for “Linear matter power spectrum  $\rightarrow$  Observables” separately is very useful and time-saving: given the common language of  $\{\alpha, \beta, \gamma\}$ , those interested in particle physics models can provide  $\{\alpha, \beta, \gamma\}$  as functions of model parameters, while those who reports observational constraints can update the constraints in terms of  $\{\alpha, \beta, \gamma\}$ . Neural network technique provides us with a ready-to-use format for this procedure.

## 5 Summary

Galactic-scale structure formation of the Universe is of particular interest in DM research. Beyond-WIMP scenarios alter galactic-scale structure formation, while conventional WIMP DM behaves as CDM. Precise measurement of galactic-scale structure in near-future observations may hint beyond-WIMP scenarios. On the other hand, here is a practical bottleneck. Impacts of beyond-WIMP scenarios on galactic-scale structure vary model by model. In principle, one has to repeat the two-step procedure on a model-by-model basis:

$$\text{Model} \rightarrow \text{Linear matter power spectrum} \rightarrow \text{Observables},$$

which is sketched by the blue flow in Fig. 1. Each step requires different disciplines and dedicated computations. Following this procedure in the model-by-model basis is very time-consuming.

We may improve the situation by characterizing the transfer function (*i.e.*, the linear matter power spectrum) with some parameter. One (likely particle physicist) calculates the transfer function parameter as a function of model parameters. Another reports observational constraints in terms of the transfer function parameter. Now we can get constraints on the model parameters very easily by combining the two results. Although a single-parameter characterization (the thermal WDM mass  $m_{\text{WDM}}$ ) has been conventionally used, 3-parameter characterization is proposed to cover a wide range of beyond-WIMP scenarios. Our main stress is that neural network technique facilitates sharing results from one side to another by providing the results in a ready-to-use format.

We devoted this paper to demonstrating how we can actually work out with  $\{\alpha, \beta, \gamma\}$  and a neural network. To be specific, we considered a simplified model of light (keV-scale)

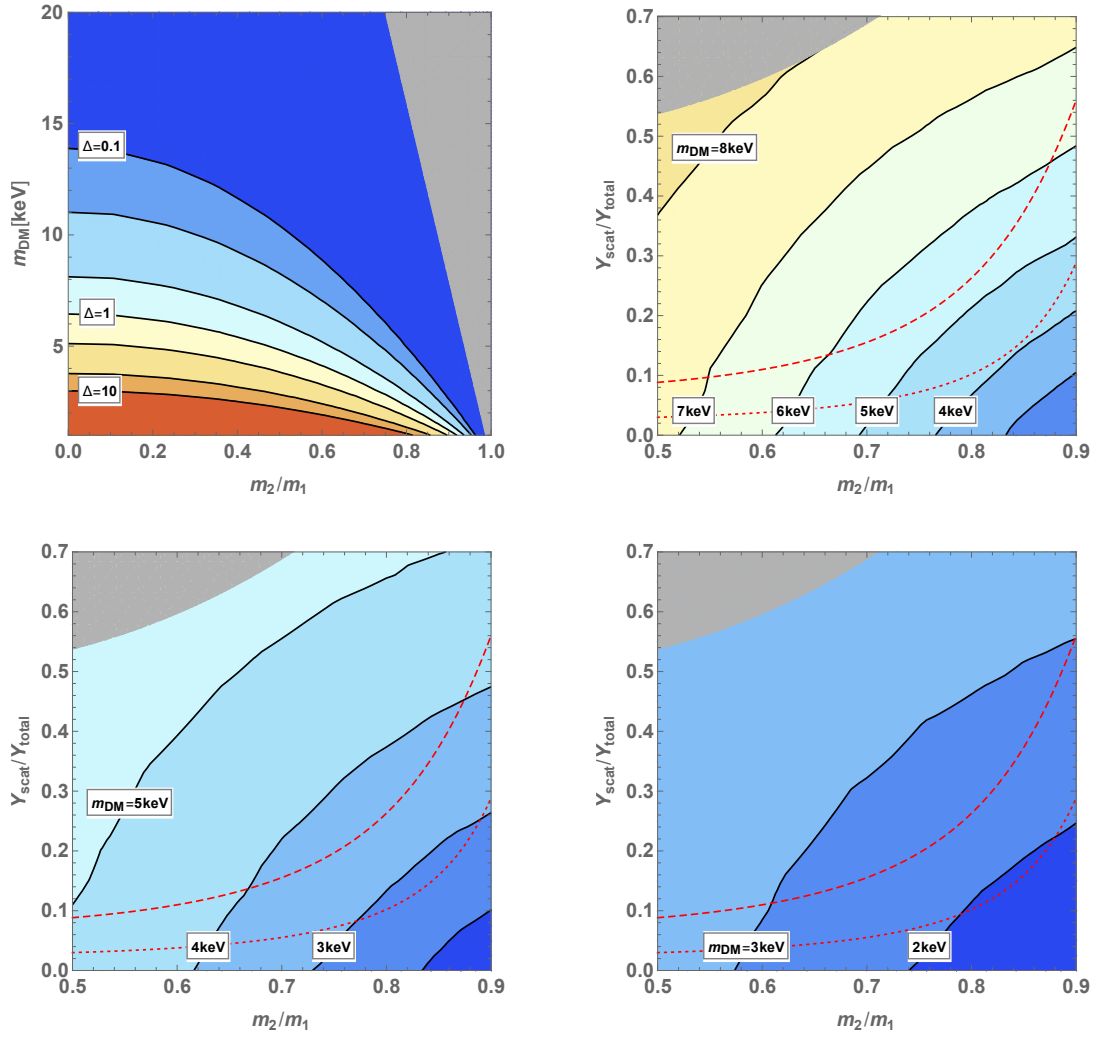


Figure 5: Constraints from  $N_{\text{sat}} > N_{\text{sat}}^{\text{obs}}$  reproduced by the neural network. Compare this figure with Fig. 2.

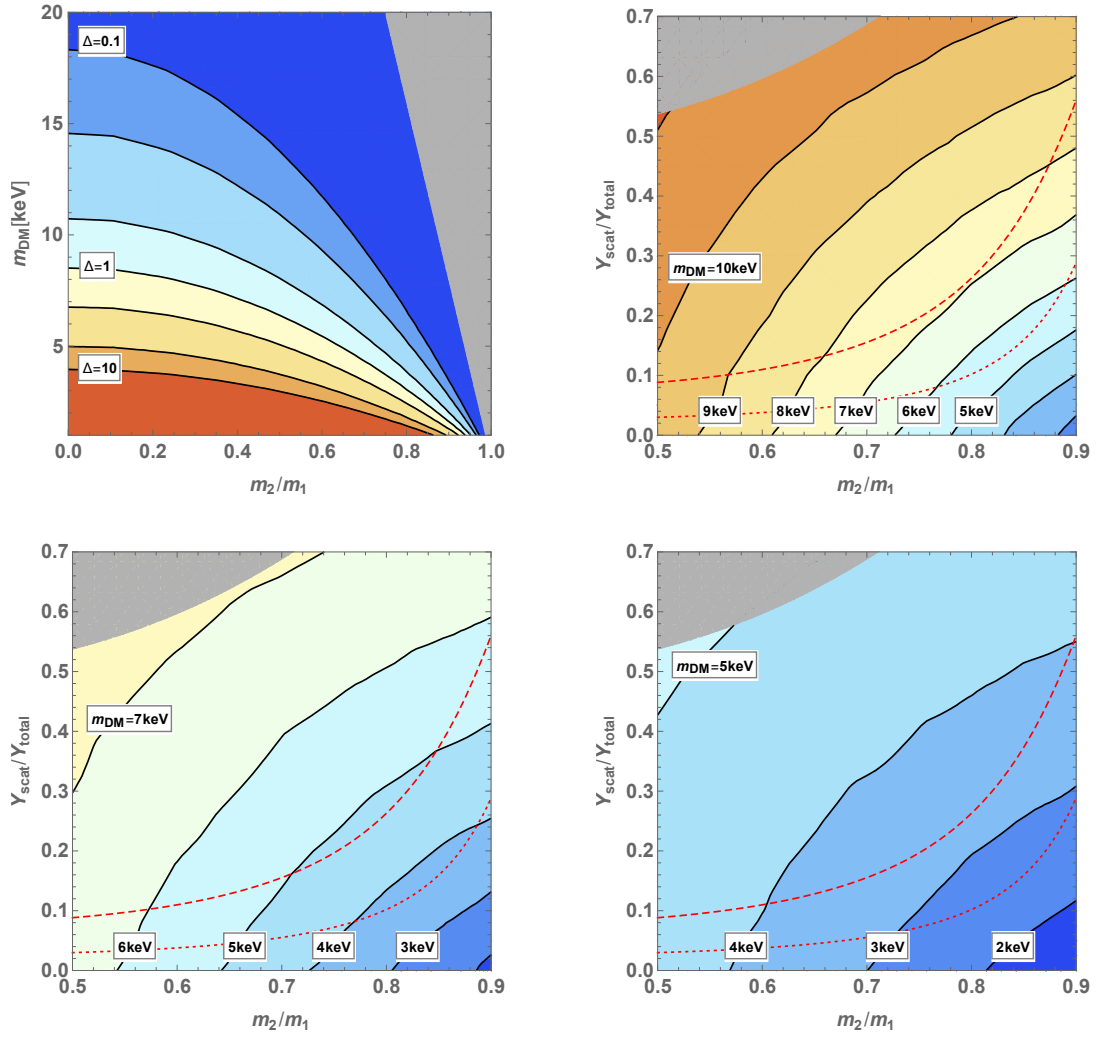


Figure 6: Constraints from  $\delta A < \delta A_{3.5 \text{ keV}}$  reproduced by the neural network. Compare this figure with Fig. 3.

FIMP DM Freeze-in production from 2-body decay gives a main contribution to the relic abundance. We also took into account entropy production after the decoupling and freeze-in production from scattering. We constructed first a map between the FIMP model parameters and  $\{\alpha, \beta, \gamma\}$  and next a map between  $\{\alpha, \beta, \gamma\}$  and the observables, *i.e.*, the number of satellite galaxies and Lyman- $\alpha$  forest, by adopting neural network technique. We provided the constructed maps in a ready-to-use format through the `arXiv` website. Meanwhile, we performed the conventional procedure to derive the direct constraints on the FIMP model parameters. The constraints derived through  $\{\alpha, \beta, \gamma\}$  and a neural network are in good agreement with those derived through the conventional procedure.

Although we focused on a simplified model of FIMP DM in this paper, it is worth performing a similar study in other FIMP models such as sterile neutrino DM and superWIMP DM and also in other alternatives to CDM such as Fuzzy DM and late kinetic decoupling of DM. Our suggestion will facilitate comparison between beyond-WIMP models and future updates of constraints on galactic-scale structure formation, *e.g.*, from redshifted 21cm surveys.

## Acknowledgments

The work of KJB, RJ, and AK was supported by IBS under the project code, IBS-R018-D1. The work of RJ was supported by Grants-in-Aid for JSPS Overseas Research Fellow (No. 201960698). The work of RJ was supported by the Deutsche Forschungsgemeinschaft under Germany's Excellence Strategy – EXC 2121 „Quantum Universe“ – 390833306. The work of KY was supported by JSPS KAKENHI Grant Number JP18J10202.

## A Comparison with an analytic map

In this appendix we derive constraints on our FIMP model parameters by converting the thermal WDM mass  $m_{\text{WDM}}$ . Proposed ways of converting  $m_{\text{WDM}}$  onto a given model are as follows:

- One compares the characteristic quantity such as the free-streaming length [201, 202] and Jeans length [203–205] between a given WDM model and the conventional thermal WDM model. If the free-streaming length in the given model is larger than that in the conventional thermal WDM model with an observational lower bound on  $m_{\text{WDM}}$ , the given model is regarded as disfavored by the same observation. See Ref. [60] for comparison of the transfer function in different WDM models with the Jeans length fixed.
- One compares the transfer function  $T^2(k)$  below some critical wavenumber between a given model and the conventional thermal WDM model. If  $T^2(k)$  in the given model is smaller in amplitude than that in the conventional thermal WDM model with a observational lower bound on  $m_{\text{WDM}}$ , the given model is regarded as disfavored by the same observation. A suggested choice of the critical wavenumber is the half mode  $k_{1/2}$  where  $T_{\text{WDM}}^2(k_{1/2}) = 1/2$  [109].

In this appendix, we adopt a “warmness” quantity (equivalently, the Jeans length) calculated from a DM phase space distribution [60]:

$$\sigma \equiv \frac{\sqrt{\langle p^2 \rangle}}{m_\chi} = \tilde{\sigma} \times \frac{T_{\text{DM}}}{m_\chi}, \quad (\text{A.1})$$

where  $\langle p^2 \rangle$  is the 2nd moment of the DM phase space distribution and thus

$$\tilde{\sigma}^2 = \frac{\int d^3q q^2 f(q)}{\int d^3q f(q)}. \quad (\text{A.2})$$

$\tilde{\sigma}$  depends on the shape of the phase space distribution. For a given observational lower bound on  $m_{\text{WDM}}$ , a WDM model is regarded as disfavored by the same observation, if  $\sigma > \sigma_{m_{\text{WDM}}}$ . Using the definition of DM temperature given by Eq. (3.2), we obtain the constraint on a FIMP as

$$m > 7 \text{ keV} \left( \frac{m_{\text{WDM}}}{2.5 \text{ keV}} \right)^{4/3} \left( \frac{\tilde{\sigma}}{3.6} \right) \left( \frac{106.75}{g_*(T_{\text{dec}})} \right)^{1/3}. \quad (\text{A.3})$$

Note that in the conventional thermal WDM model, WDM particles follows the Fermi-Dirac distribution, and thus  $\tilde{\sigma}_{\text{WDM}} \simeq 3.6$ .

In our simplified FIMP model, the phase space distribution can be expressed analytically [206], and thus  $\tilde{\sigma}$  is also analytically derivable. As a result, we can construct an analytic map between  $m_{\text{WDM}}$  and the model parameters. The total  $\tilde{\sigma}$  is calculated from each production process as

$$\tilde{\sigma}^2 = \frac{Y_{\text{dec}}}{Y_{\text{total}}} \tilde{\sigma}_{\text{dec}}^2 + \frac{Y_{\text{scat, t-ch}}}{Y_{\text{total}}} \tilde{\sigma}_{\text{scat, t-ch}}^2 + \frac{Y_{\text{scat, s-ch}}}{Y_{\text{total}}} \tilde{\sigma}_{\text{scat, s-ch}}^2, \quad (\text{A.4})$$

where each  $\tilde{\sigma}^2$  is calculated analytically as

$$\tilde{\sigma}_{\text{dec}}^2 = \frac{35}{4}(1 - r^2)^2, \quad (\text{A.5})$$

$$\tilde{\sigma}_{\text{scat, t-ch}}^2 = \frac{35}{4}, \quad (\text{A.6})$$

$$\tilde{\sigma}_{\text{scat, s-ch}}^2 = \frac{7(105r - 265r^3 + 191r^5 - 15r^7 - 15(1 - r^2)^3(7 + r^2) \tanh^{-1} r)}{12r^4(r(3 - r^2) + (-3 + 2r^2 + r^4) \tanh^{-1} r)}, \quad (\text{A.7})$$

and each FIMP yield is also obtained as

$$Y_{\text{dec}} = 2 \times \frac{3y_\chi^2 M_0}{32\pi^2 m_\Psi} (1 - r^2)^2, \quad (\text{A.8})$$

$$Y_{\text{scat, t-ch}} = 4 \times \frac{3N_f y_\chi^2 y_f^2 M_0}{128\pi^4 m_\Psi} \cdot \frac{(2 - r^2) \tanh^{-1} \sqrt{1 - r^2} - \sqrt{1 - r^2}}{3(1 - r^2)^{3/2}}, \quad (\text{A.9})$$

$$Y_{\text{scat, s-ch}} = 2 \times \frac{3N_f y_\chi^2 y_f^2 M_0}{128\pi^4 m_\Psi} \cdot \frac{r(3 - r^2) + (-3 + 2r^2 + r^4) \tanh^{-1}(r)}{2r^5}. \quad (\text{A.10})$$

Here  $r \equiv m_2/m_1$ , prefactors count a number of particle species ( $\Psi/\bar{\Psi}$  and  $f/\bar{f}$ ), and  $M_0$  is a dimensionful constant whose expression is not relevant in this appendix.

In this way, we derive the constraints on our simplified FIMP model from  $m_{\text{WDM}}$  through warmness. First, Fig. 7 shows constraints from the observed number of Milky Way satellites,  $\sigma > \sigma_{2.9 \text{ keV}}$ .  $m_{\text{WDM}} > 2.9 \text{ keV}$  corresponds to  $N_{\text{sat}} > N_{\text{sat}}^{\text{obs}}$ . The left and right panels are for Case A (Decay with entropy production) and Case B (Decay with scattering) with  $\Delta = 1$  and should be compared with the top-left and top-right panels of Fig. 2, respectively. We see the results are  $\sim 10\%$  different with each other, while are qualitatively equivalent.

Next, Fig. 8 shows constraints from the Lyman- $\alpha$  forest data,  $\sigma > \sigma_{3.5 \text{ keV}}$ .  $m_{\text{WDM}} > 3.5 \text{ keV}$  corresponds to  $\delta A < \delta A_{3.5 \text{ keV}}$ . The left and right panels are for Case A and Case B with  $\Delta = 1$  and should be compared with the top-left and top-right panels of Fig. 3, respectively. We see the derived results are  $\sim 10\%$  different from those from the direct modeling in Sec. 3.2, as for  $N_{\text{sat}} > N_{\text{sat}}^{\text{obs}}$ .<sup>◇14</sup>

## B Further check: original data vs neural network

In this appendix, we take a closer look at the difference between the original data and neural network.

First we check validity of the  $\{\alpha, \beta, \gamma\}$  parametrization itself (which is irrelevant to the precision of the neural network). Fig. 9 shows the transfer function for Case A with  $m_2/m_1 = 0.499$ ,  $m_{\text{DM}} = 10.256 \text{ keV}$ , and  $\Delta = 1$  (left panel) and Case B with  $m_2/m_1 = 0.701$ ,  $Y_{\text{scat}}/Y_{\text{tot}} = 0.367$ ,  $m_{\text{DM}} = 4 \text{ keV}$ , and  $\Delta = 1$  (right panel). The red points are data points, while the blue lines are  $T^2(k)$  given by Eq. (2.14) with the fitted values of  $\{\alpha, \beta, \gamma\}$  ( $\gamma = -\beta$

<sup>◇14</sup> We also derive the constraints through  $k_{1/2}$ . The derived constraints are again  $\sim 10\%$  different from those from the direct modeling.

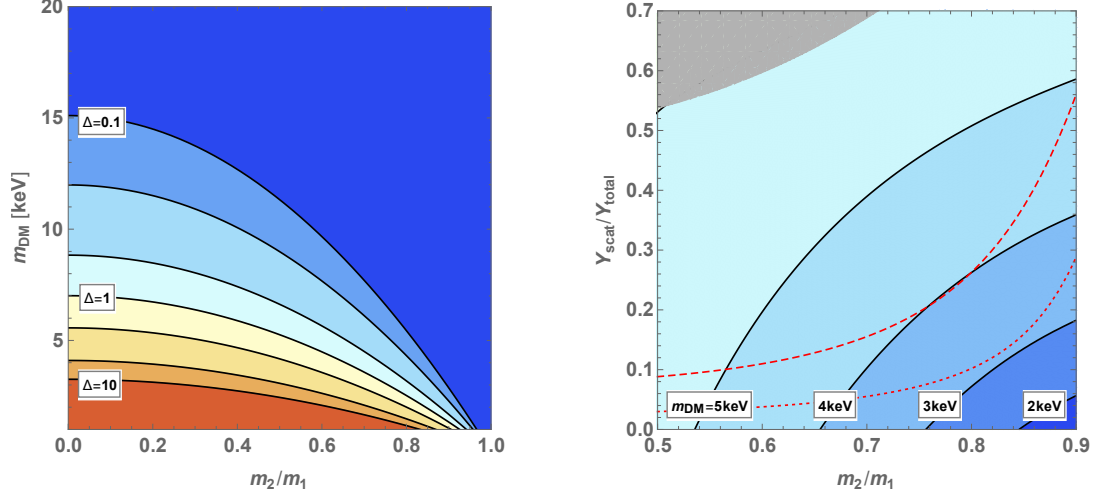


Figure 7: Constraints on Case A (left) and Case B with  $\Delta = 1$  (right) from  $\sigma < \sigma_{2.9\text{keV}}$ , where  $\sigma_{2.9\text{keV}}$  denotes the warmness of 2.9 keV conventional WDM. The left and right panels should be compared with the top-left and bottom-left panels of Fig. 2, respectively.

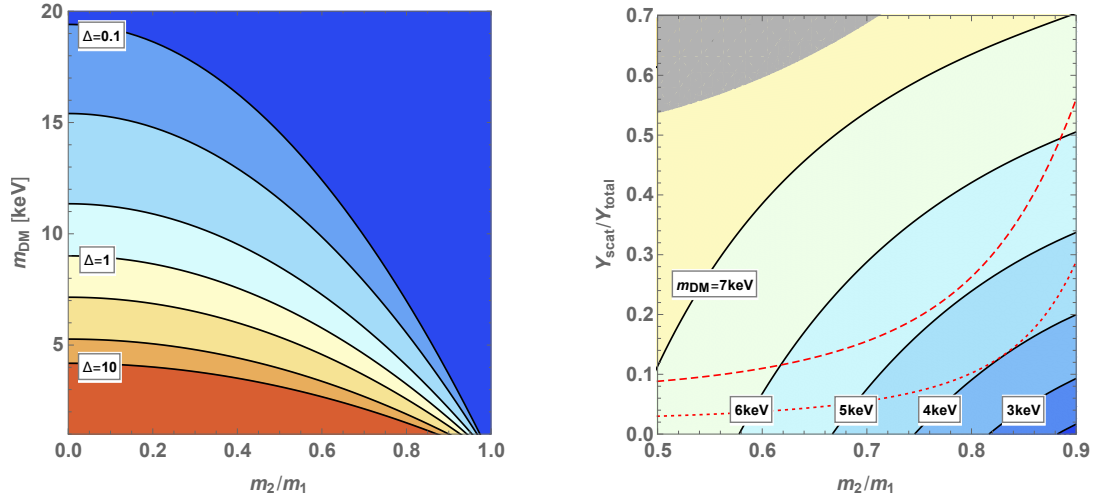


Figure 8: Constraints on Case A (left) and Case B with  $\Delta = 1$  (right) from  $\sigma < \sigma_{3.5\text{keV}}$ , where  $\sigma_{3.5\text{keV}}$  denotes the warmness of 3.5 keV conventional WDM. This figure should be compared with the top-left and bottom-left panels of Fig. 3.



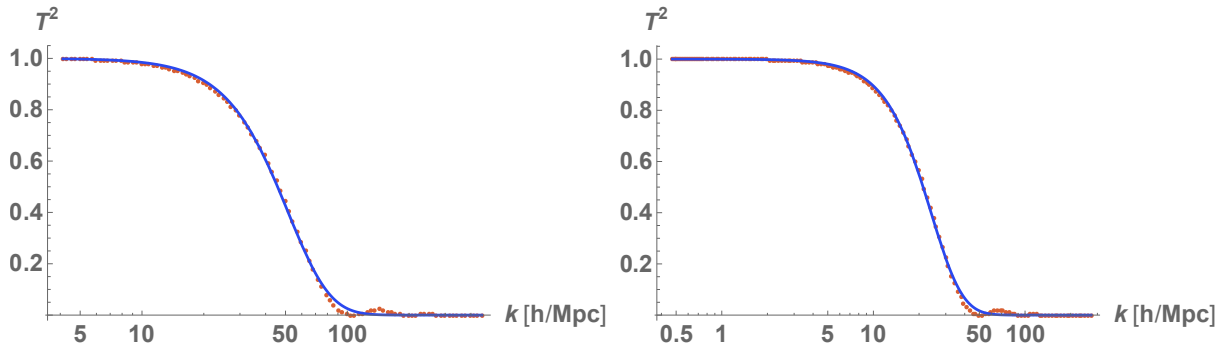


Figure 9: Comparison between original data (red) and fitting function with  $\alpha$  and  $\beta$  given by the neural network (blue). We show two benchmark points. **Left:** Case A (Decay with entropy production) with  $m_2/m_1 = 0.499$ ,  $m_{\text{DM}} = 10.256$  keV, and  $\Delta = 1$ . **Right:** Case B (Decay with scattering) with  $m_2/m_1 = 0.701$ ,  $Y_{\text{scat}}/Y_{\text{tot}} = 0.367$ ,  $m_{\text{DM}} = 4$  keV, and  $\Delta = 1$ .

as explained in Sec. 4.2). We see that the  $\{\alpha, \beta, \gamma\}$  parametrization nicely reproduces the original data.

Next we examine the precision of the neural network. Fig. 10 compares the original values of  $\alpha$  and  $\beta$  (upper panels) and the fit from the neural network (lower panels) for Case A with  $\Delta = 1$ . Similarly, Fig. 11 is for Case B with  $m_{\text{DM}} = 4$  keV. We see that the neural network not only reproduces the original data quite well, but also somewhat smoothens artificial fluctuations in the original data.

Figs. 12 and 13 are color plots for the relative error between the original data and neural network for  $\alpha$  (left columns) and  $\beta$  (right columns), respectively. Fig. 12 is for Case A with  $\Delta = 0.1, 1, \text{ and } 10$  from top to bottom, while Fig. 13 is for Case B with  $m_{\text{DM}} = 2, 4, \text{ and } 6$  keV for  $\Delta = 1$  from top to bottom. The relative error for Case A is at most 1% in  $\alpha$  and  $\beta$ , while for Case B the error is at most 2% and 0.2% in  $\alpha$  and  $\beta$ , respectively.

We finally comment that the error of the neural network for “ $\{\alpha, \beta, \gamma\} \rightarrow \text{Observables}$ ” is much smaller than that for “Model parameters  $\rightarrow \{\alpha, \beta, \gamma\}$ ”.

## C How to use the neural network data

In this appendix we explain how to use the data provided through the `arXiv` website. The datafile we provide are

- `mean.tsv`, `std.tsv`,
- `b1.tsv`, `b2.tsv`, `bout.tsv`,
- `w1.tsv`, `w2.tsv`, `wout.tsv`.

The first items are the means,  $\vec{x}_0 \equiv (\vec{x}_{\text{in},0}^T, \vec{x}_{\text{out},0}^T)^T$ , and standard deviations,  $\vec{\sigma} \equiv (\vec{\sigma}_{\text{in}}^T, \vec{\sigma}_{\text{out}}^T)^T$ , which shift and normalize the neural network input and output. The second items are the biases,  $\vec{b}_1$ ,  $\vec{b}_2$ , and  $\vec{b}_{\text{out}}$ , while the last items are the weight matrices,  $W_1$ ,  $W_2$ , and  $W_{\text{out}}$ .

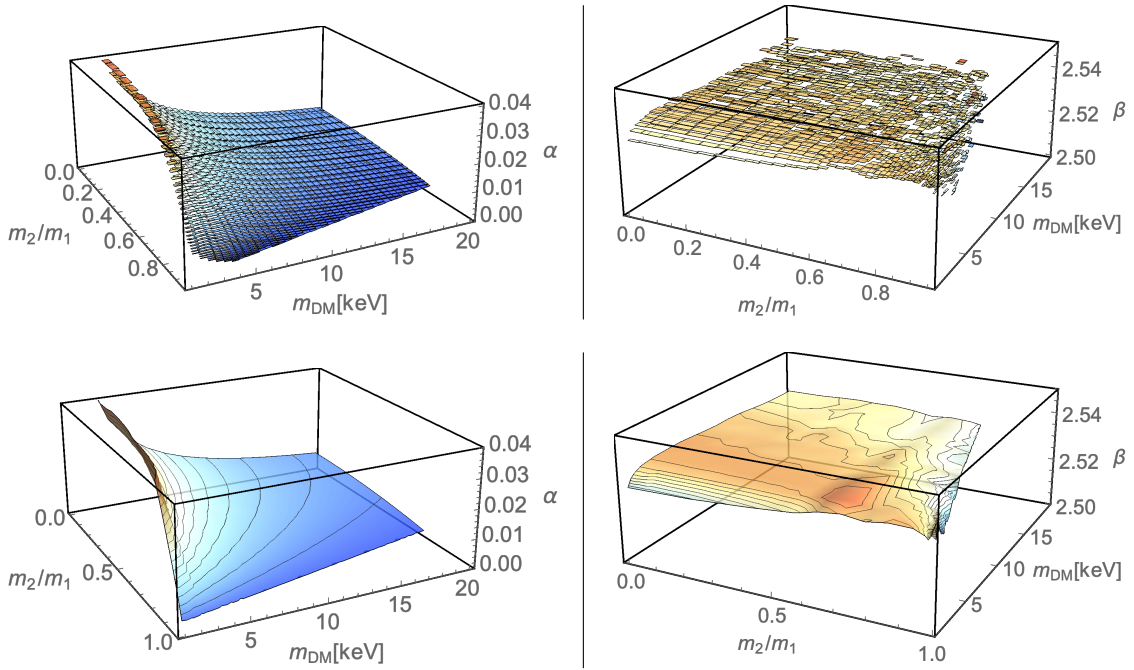


Figure 10: Original data (upper) and functional forms learned by the neural network (lower) for  $\Delta = 1$ . The left and right columns correspond to  $\alpha$  and  $\beta$ , respectively.

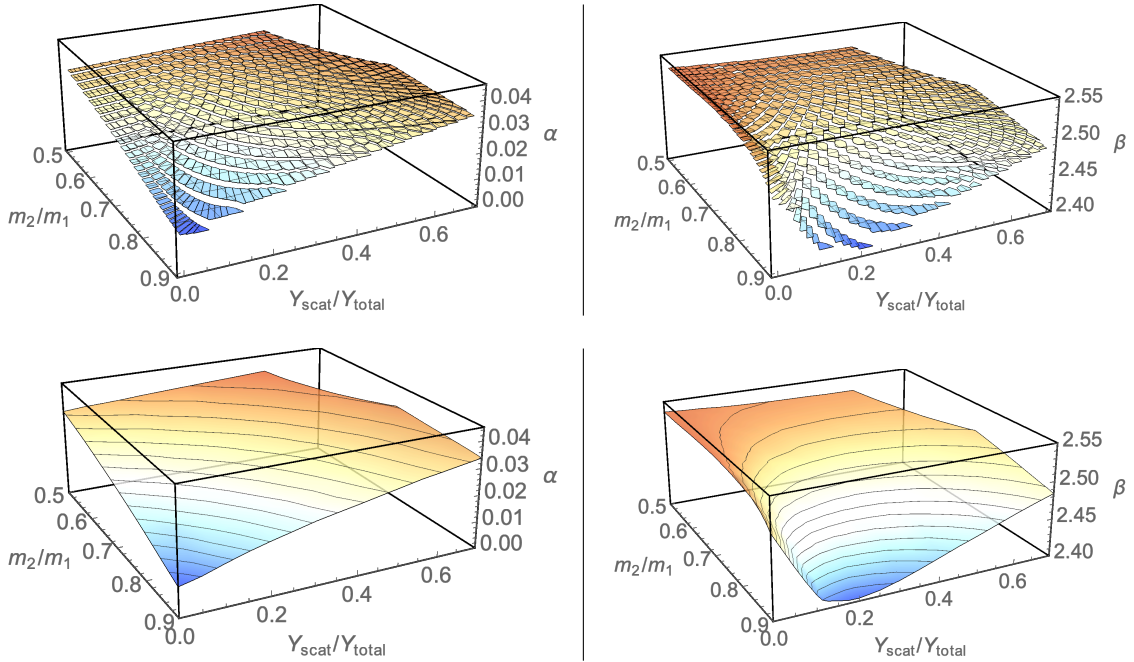


Figure 11: Original data (upper) and functional forms learned by the neural network (lower) for  $m_{\text{DM}} = 4 \text{ keV}$ . The left and right columns correspond to  $\alpha$  and  $\beta$ , respectively.

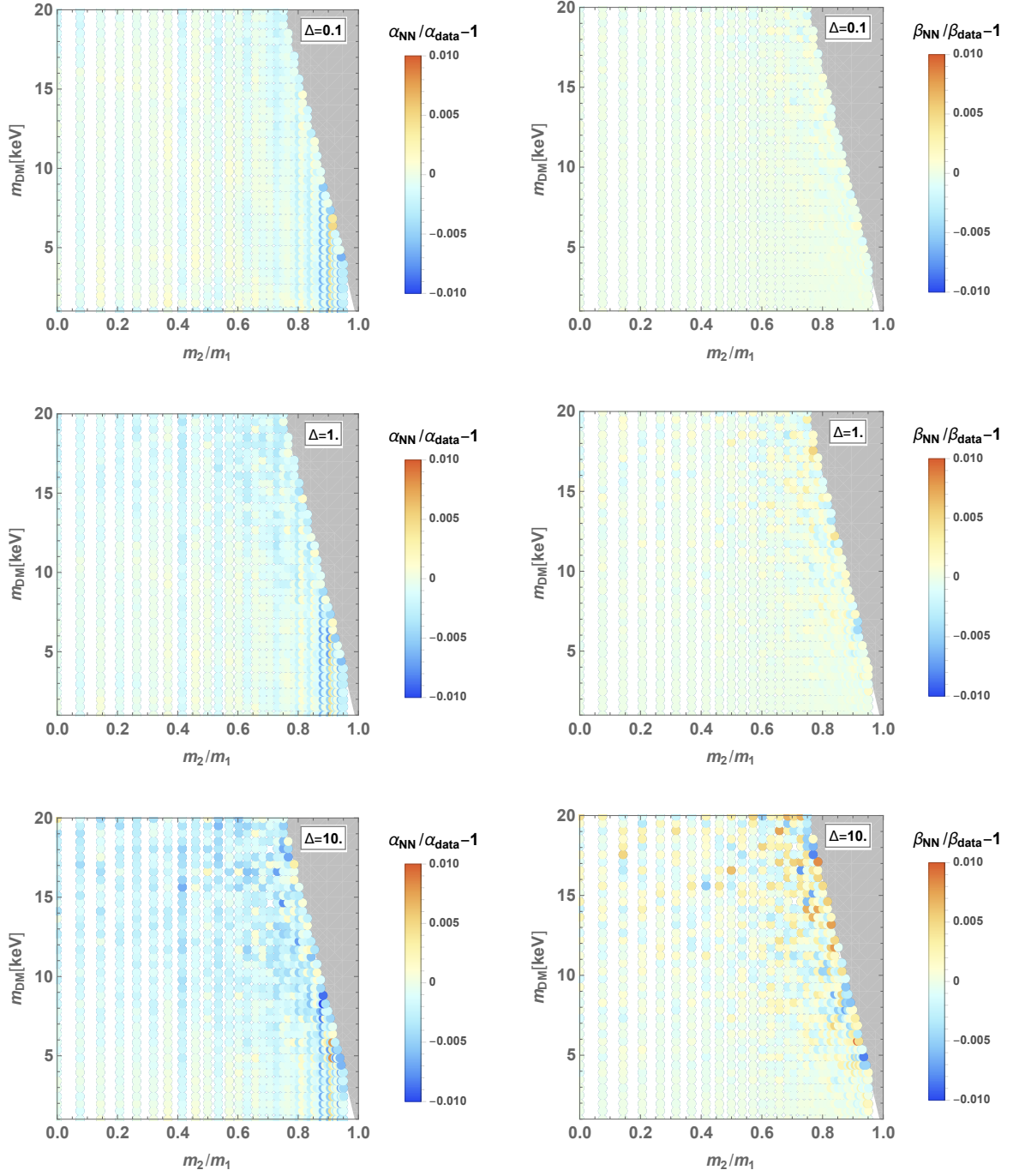


Figure 12: Relative error between  $\alpha$  (left) or  $\beta$  (right) obtained from the original data and those learned by the neural network. This figure is for Case A (Decay with entropy production). We show  $\Delta = 0.1$  (top), 1 (middle), and 10 (bottom).

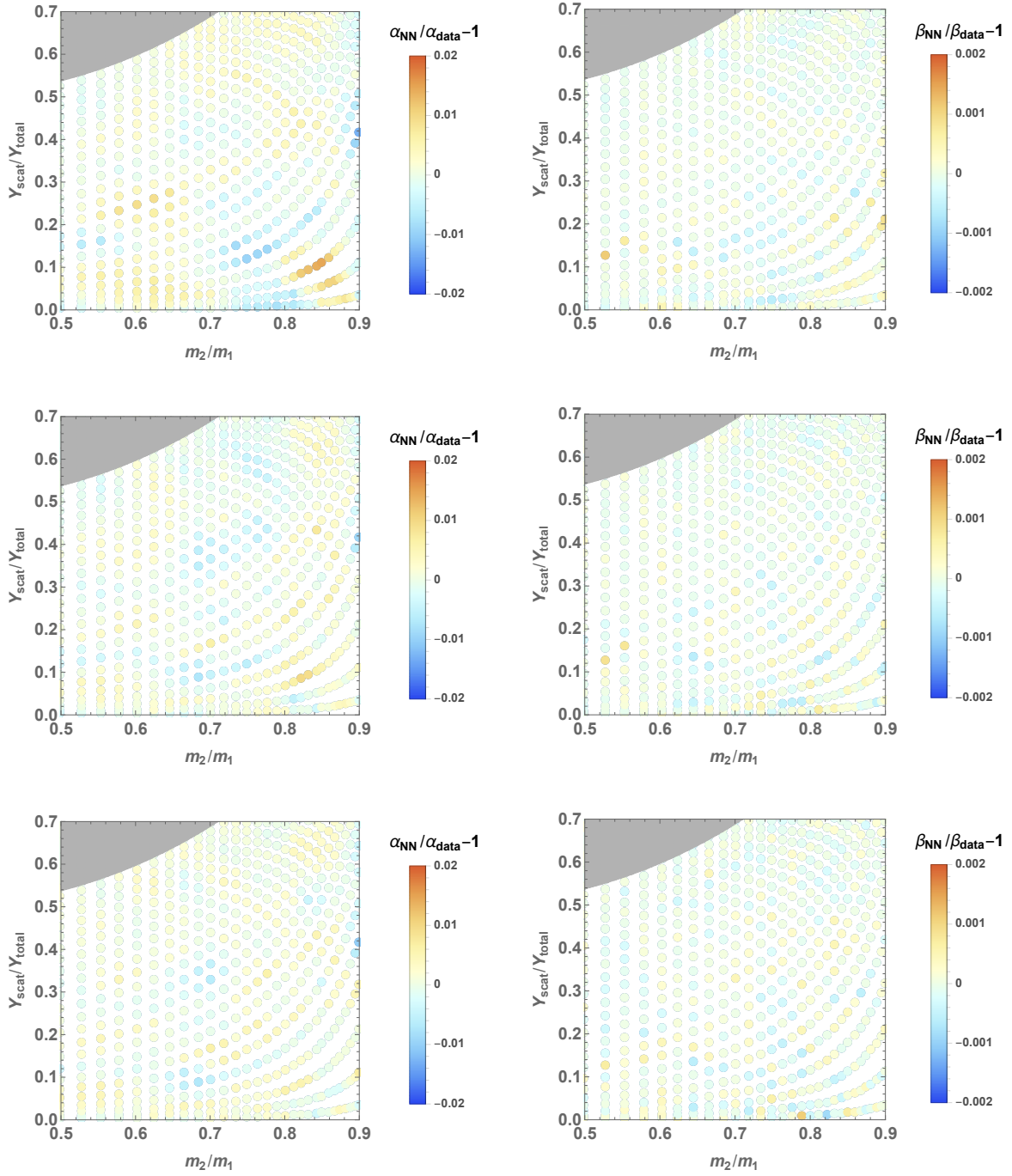


Figure 13: Relative error between  $\alpha$  (left) or  $\beta$  (right) obtained from the original data and those learned by the neural network. This figure is for Case B (Decay with scattering). We show  $\Delta = 1$  with  $m_{\text{DM}} = 2$  (top), 4 (middle), and 6 keV (bottom).

The data files for “Model parameters  $\rightarrow \{\alpha, \beta, \gamma\}$ ” are in the directory of `freeze-in/CaseA` for Case A, and in `freeze-in/CaseB/Delta=...` for Case B, respectively. The data files for “ $\{\alpha, \beta, \gamma\} \rightarrow$  Observables” are in `freeze-in/NSat` and `freeze-in/deltaA` for  $N_{\text{sat}}$  and  $\delta A$ , respectively.

## References

- [1] J. L. Feng, “Dark Matter Candidates from Particle Physics and Methods of Detection,” *Ann. Rev. Astron. Astrophys.* **48** (2010) 495–545, [arXiv:1003.0904 \[astro-ph.CO\]](#).
- [2] G. Arcadi, M. Dutra, P. Ghosh, M. Lindner, Y. Mambrini, M. Pierre, S. Profumo, and F. S. Queiroz, “The waning of the WIMP? A review of models, searches, and constraints,” *Eur. Phys. J.* **C78** no. 3, (2018) 203, [arXiv:1703.07364 \[hep-ph\]](#).
- [3] L. Roszkowski, E. M. Sessolo, and S. Trojanowski, “WIMP dark matter candidates and searches—current status and future prospects,” *Rept. Prog. Phys.* **81** no. 6, (2018) 066201, [arXiv:1707.06277 \[hep-ph\]](#).
- [4] **ATLAS** Collaboration, M. Aaboud *et al.*, “Search for dark matter and other new phenomena in events with an energetic jet and large missing transverse momentum using the ATLAS detector,” *JHEP* **01** (2018) 126, [arXiv:1711.03301 \[hep-ex\]](#).
- [5] **CMS** Collaboration, A. M. Sirunyan *et al.*, “Search for new physics in final states with an energetic jet or a hadronically decaying  $W$  or  $Z$  boson and transverse momentum imbalance at  $\sqrt{s} = 13$  TeV,” *Phys. Rev.* **D97** no. 9, (2018) 092005, [arXiv:1712.02345 \[hep-ex\]](#).
- [6] **XENON** Collaboration, E. Aprile *et al.*, “Dark Matter Search Results from a One Ton-Year Exposure of XENON1T,” *Phys. Rev. Lett.* **121** no. 11, (2018) 111302, [arXiv:1805.12562 \[astro-ph.CO\]](#).
- [7] **PandaX-II** Collaboration, X. Cui *et al.*, “Dark Matter Results From 54-Ton-Day Exposure of PandaX-II Experiment,” *Phys. Rev. Lett.* **119** no. 18, (2017) 181302, [arXiv:1708.06917 \[astro-ph.CO\]](#).
- [8] **PICO** Collaboration, C. Amole *et al.*, “Dark Matter Search Results from the Complete Exposure of the PICO-60  $\text{C}_3\text{F}_8$  Bubble Chamber,” [arXiv:1902.04031 \[astro-ph.CO\]](#).
- [9] **MAGIC**, **Fermi-LAT** Collaboration, M. L. Ahnen *et al.*, “Limits to Dark Matter Annihilation Cross-Section from a Combined Analysis of MAGIC and Fermi-LAT Observations of Dwarf Satellite Galaxies,” *JCAP* **1602** no. 02, (2016) 039, [arXiv:1601.06590 \[astro-ph.HE\]](#).
- [10] M. R. Buckley and A. H. G. Peter, “Gravitational probes of dark matter physics,” [arXiv:1712.06615 \[astro-ph.CO\]](#).
- [11] **Planck** Collaboration, N. Aghanim *et al.*, “Planck 2018 results. VI. Cosmological parameters,” [arXiv:1807.06209 \[astro-ph.CO\]](#).

- [12] **BOSS** Collaboration, S. Alam *et al.*, “The clustering of galaxies in the completed SDSS-III Baryon Oscillation Spectroscopic Survey: cosmological analysis of the DR12 galaxy sample,” *Mon. Not. Roy. Astron. Soc.* **470** no. 3, (2017) 2617–2652, [arXiv:1607.03155 \[astro-ph.CO\]](#).
- [13] A. A. Klypin, A. V. Kravtsov, O. Valenzuela, and F. Prada, “Where are the missing Galactic satellites?,” *Astrophys. J.* **522** (1999) 82–92, [arXiv:astro-ph/9901240 \[astro-ph\]](#).
- [14] B. Moore, S. Ghigna, F. Governato, G. Lake, T. R. Quinn, J. Stadel, and P. Tozzi, “Dark matter substructure within galactic halos,” *Astrophys. J.* **524** (1999) L19–L22, [arXiv:astro-ph/9907411 \[astro-ph\]](#).
- [15] J. Zavala, Y. P. Jing, A. Faltenbacher, G. Yepes, Y. Hoffman, S. Gottlober, and B. Catinella, “The velocity function in the local environment from LCDM and LWDM constrained simulations,” *Astrophys. J.* **700** (2009) 1779–1793, [arXiv:0906.0585 \[astro-ph.CO\]](#).
- [16] E. Papastergis, A. M. Martin, R. Giovanelli, and M. P. Haynes, “The velocity width function of galaxies from the 40% ALFALFA survey: shedding light on the cold dark matter overabundance problem,” *Astrophys. J.* **739** (2011) 38, [arXiv:1106.0710 \[astro-ph.CO\]](#).
- [17] A. Klypin, I. Karachentsev, D. Makarov, and O. Nasonova, “Abundance of Field Galaxies,” *Mon. Not. Roy. Astron. Soc.* **454** no. 2, (2015) 1798–1810, [arXiv:1405.4523 \[astro-ph.CO\]](#).
- [18] R. A. Flores and J. R. Primack, “Observational and theoretical constraints on singular dark matter halos,” *Astrophys. J.* **427** (1994) L1–4, [arXiv:astro-ph/9402004 \[astro-ph\]](#).
- [19] B. Moore, “Evidence against dissipationless dark matter from observations of galaxy haloes,” *Nature* **370** (1994) 629.
- [20] B. Moore, T. R. Quinn, F. Governato, J. Stadel, and G. Lake, “Cold collapse and the core catastrophe,” *Mon. Not. Roy. Astron. Soc.* **310** (1999) 1147–1152, [arXiv:astro-ph/9903164 \[astro-ph\]](#).
- [21] S.-H. Oh *et al.*, “High-resolution mass models of dwarf galaxies from LITTLE THINGS,” *Astron. J.* **149** (2015) 180, [arXiv:1502.01281 \[astro-ph.GA\]](#).
- [22] M. Boylan-Kolchin, J. S. Bullock, and M. Kaplinghat, “Too big to fail? The puzzling darkness of massive Milky Way subhaloes,” *Mon. Not. Roy. Astron. Soc.* **415** (2011) L40, [arXiv:1103.0007 \[astro-ph.CO\]](#).
- [23] M. Boylan-Kolchin, J. S. Bullock, and M. Kaplinghat, “The Milky Way’s bright satellites as an apparent failure of LCDM,” *Mon. Not. Roy. Astron. Soc.* **422** (2012) 1203–1218, [arXiv:1111.2048 \[astro-ph.CO\]](#).
- [24] I. Ferrero, M. G. Abadi, J. F. Navarro, L. V. Sales, and S. Gurovich, “The dark matter halos of dwarf galaxies: a challenge for the LCDM paradigm?,” *Mon. Not. Roy. Astron. Soc.* **425** (2012) 2817–2823, [arXiv:1111.6609 \[astro-ph.CO\]](#).

- [25] E. J. Tollerud, M. Boylan-Kolchin, and J. S. Bullock, “M31 Satellite Masses Compared to LCDM Subhaloes,” *Mon. Not. Roy. Astron. Soc.* **440** no. 4, (2014) 3511–3519, [arXiv:1403.6469 \[astro-ph.GA\]](#).
- [26] S. Garrison-Kimmel, M. Boylan-Kolchin, J. S. Bullock, and E. N. Kirby, “Too Big to Fail in the Local Group,” *Mon. Not. Roy. Astron. Soc.* **444** no. 1, (2014) 222–236, [arXiv:1404.5313 \[astro-ph.GA\]](#).
- [27] E. Papastergis, R. Giovanelli, M. P. Haynes, and F. Shankar, “Is there a “too big to fail” problem in the field?,” *Astron. Astrophys.* **574** (2015) A113, [arXiv:1407.4665 \[astro-ph.GA\]](#).
- [28] J. S. Bullock and M. Boylan-Kolchin, “Small-Scale Challenges to the  $\Lambda$ CDM Paradigm,” *Ann. Rev. Astron. Astrophys.* **55** (2017) 343–387, [arXiv:1707.04256 \[astro-ph.CO\]](#).
- [29] F. Governato *et al.*, “At the heart of the matter: the origin of bulgeless dwarf galaxies and Dark Matter cores,” *Nature* **463** (2010) 203–206, [arXiv:0911.2237 \[astro-ph.CO\]](#).
- [30] F. Governato, A. Zolotov, A. Pontzen, C. Christensen, S. H. Oh, A. M. Brooks, T. Quinn, S. Shen, and J. Wadsley, “Cuspy No More: How Outflows Affect the Central Dark Matter and Baryon Distribution in Lambda CDM Galaxies,” *Mon. Not. Roy. Astron. Soc.* **422** (2012) 1231–1240, [arXiv:1202.0554 \[astro-ph.CO\]](#).
- [31] A. Zolotov, A. M. Brooks, B. Willman, F. Governato, A. Pontzen, C. Christensen, A. Dekel, T. Quinn, S. Shen, and J. Wadsley, “Baryons Matter: Why Luminous Satellite Galaxies Have Reduced Central Masses,” *Astrophys. J.* **761** (2012) 71, [arXiv:1207.0007 \[astro-ph.CO\]](#).
- [32] A. M. Brooks and A. Zolotov, “Why Baryons Matter: The Kinematics of Dwarf Spheroidal Satellites,” *Astrophys. J.* **786** (2014) 87, [arXiv:1207.2468 \[astro-ph.CO\]](#).
- [33] F. Munshi, F. Governato, A. M. Brooks, C. Christensen, S. Shen, S. Loebman, B. Moster, T. Quinn, and J. Wadsley, “Reproducing the Stellar Mass/Halo Mass Relation in Simulated LCDM Galaxies: Theory vs Observational Estimates,” *Astrophys. J.* **766** (2013) 56, [arXiv:1209.1389 \[astro-ph.CO\]](#).
- [34] A. Pontzen and F. Governato, “Cold dark matter heats up,” *Nature* **506** (2014) 171–178, [arXiv:1402.1764 \[astro-ph.CO\]](#).
- [35] P. Madau, S. Shen, and F. Governato, “Dark Matter Heating and Early Core Formation in Dwarf Galaxies,” *Astrophys. J.* **789** (2014) L17, [arXiv:1405.2577 \[astro-ph.GA\]](#).
- [36] T. Sawala *et al.*, “Local Group galaxies emerge from the dark,” [arXiv:1412.2748 \[astro-ph.GA\]](#).
- [37] T. K. Chan, D. Kereš, J. Oñorbe, P. F. Hopkins, A. L. Muratov, C. A. Faucher-Giguère, and E. Quataert, “The impact of baryonic physics on the structure of dark matter haloes: the view from the FIRE cosmological simulations,” *Mon. Not. Roy. Astron. Soc.* **454** no. 3, (2015) 2981–3001, [arXiv:1507.02282 \[astro-ph.GA\]](#).

- [38] E. Tollet *et al.*, “NIHAO – IV: core creation and destruction in dark matter density profiles across cosmic time,” *Mon. Not. Roy. Astron. Soc.* **456** no. 4, (2016) 3542–3552, [arXiv:1507.03590 \[astro-ph.GA\]](#).
- [39] T. Sawala *et al.*, “The APOSTLE simulations: solutions to the Local Group’s cosmic puzzles,” *Mon. Not. Roy. Astron. Soc.* **457** no. 2, (2016) 1931–1943, [arXiv:1511.01098 \[astro-ph.GA\]](#).
- [40] A. A. Dutton, A. V. Macciò, J. Frings, L. Wang, G. S. Stinson, C. Penzo, and X. Kang, “NIHAO V: too big does not fail – reconciling the conflict between  $\Lambda$ CDM predictions and the circular velocities of nearby field galaxies,” *Mon. Not. Roy. Astron. Soc.* **457** no. 1, (2016) L74–L78, [arXiv:1512.00453 \[astro-ph.GA\]](#).
- [41] A. R. Wetzel, P. F. Hopkins, J.-h. Kim, C.-A. Faucher-Giguere, D. Keres, and E. Quataert, “Reconciling dwarf galaxies with  $\Lambda$ CDM cosmology: Simulating a realistic population of satellites around a Milky Way-mass galaxy,” *Astrophys. J.* **827** no. 2, (2016) L23, [arXiv:1602.05957 \[astro-ph.GA\]](#).
- [42] A. V. Macciò, S. M. Udrescu, A. A. Dutton, A. Obreja, L. Wang, G. R. Stinson, and X. Kang, “NIHAO X: reconciling the local galaxy velocity function with cold dark matter via mock HI observations,” *Mon. Not. Roy. Astron. Soc.* **463** no. 1, (2016) L69–L73, [arXiv:1607.01028 \[astro-ph.GA\]](#).
- [43] A. Fattahi, J. F. Navarro, T. Sawala, C. S. Frenk, L. V. Sales, K. Oman, M. Schaller, and J. Wang, “The cold dark matter content of Galactic dwarf spheroidals: no cores, no failures, no problem,” [arXiv:1607.06479 \[astro-ph.GA\]](#).
- [44] A. M. Brooks, E. Papastergis, C. R. Christensen, F. Governato, A. Stilp, T. R. Quinn, and J. Wadsley, “How to Reconcile the Observed Velocity Function of Galaxies with Theory,” *Astrophys. J.* **850** no. 1, (2017) 97, [arXiv:1701.07835 \[astro-ph.GA\]](#).
- [45] R. Verbeke, E. Papastergis, A. A. Ponomareva, S. Rathi, and S. De Rijcke, “A new astrophysical solution to the Too Big To Fail problem,” *Astron. Astrophys.* **607** (2017) A13, [arXiv:1703.03810 \[astro-ph.GA\]](#).
- [46] A. A. Dutton, A. V. Macciò, T. Buck, K. L. Dixon, M. Blank, and A. Obreja, “NIHAO XX: The impact of the star formation threshold on the cusp-core transformation of cold dark matter haloes,” [arXiv:1811.10625 \[astro-ph.GA\]](#).
- [47] K. A. Oman *et al.*, “The unexpected diversity of dwarf galaxy rotation curves,” *Mon. Not. Roy. Astron. Soc.* **452** no. 4, (2015) 3650–3665, [arXiv:1504.01437 \[astro-ph.GA\]](#).
- [48] M. S. Pawlowski, B. Famaey, D. Merritt, and P. Kroupa, “On the persistence of two small-scale problems in  $\Lambda$ CDM,” *Astrophys. J.* **815** no. 1, (2015) 19, [arXiv:1510.08060 \[astro-ph.GA\]](#).
- [49] E. Papastergis and F. Shankar, “An assessment of the “too big to fail” problem for field dwarf galaxies in view of baryonic feedback effects,” *Astron. Astrophys.* **591** (June, 2016) A58, [arXiv:1511.08741](#).



- [50] K. A. Oman, J. F. Navarro, L. V. Sales, A. Fattahi, C. S. Frenk, T. Sawala, M. Schaller, and S. D. M. White, “Missing dark matter in dwarf galaxies?,” *Mon. Not. Roy. Astron. Soc.* **460** no. 4, (2016) 3610–3623, [arXiv:1601.01026 \[astro-ph.GA\]](#).
- [51] L. V. Sales *et al.*, “The low-mass end of the baryonic Tully-Fisher relation,” *Mon. Not. Roy. Astron. Soc.* **464** no. 2, (2017) 2419–2428, [arXiv:1602.02155 \[astro-ph.GA\]](#).
- [52] S. Trujillo-Gomez, A. Schneider, E. Papastergis, D. S. Reed, and G. Lake, “Another baryon miracle? Testing solutions to the ‘missing dwarfs’ problem,” *Mon. Not. Roy. Astron. Soc.* **475** no. 4, (2018) 4825–4840, [arXiv:1610.09335 \[astro-ph.CO\]](#).
- [53] S. Garrison-Kimmel, P. F. Hopkins, A. Wetzel, J. S. Bullock, M. Boylan-Kolchin, D. Keres, C.-A. Faucher-Giguere, K. El-Badry, A. Lamberts, E. Quataert, and R. Sanderson, “The Local Group on FIRE: Dwarf galaxy populations across a suite of hydrodynamic simulations,” *arXiv e-prints* (June, 2018) , [arXiv:1806.04143](#).
- [54] S. Bose *et al.*, “No cores in dark matter-dominated dwarf galaxies with bursty star formation histories,” [arXiv:1810.03635 \[astro-ph.GA\]](#).
- [55] A. Benitez-Llambay, C. S. Frenk, A. D. Ludlow, and J. F. Navarro, “Baryon-induced dark matter cores in the EAGLE simulations,” *arXiv e-prints* (Oct., 2018) , [arXiv:1810.04186](#).
- [56] V. Avila-Reese, P. Colin, O. Valenzuela, E. D’Onghia, and C. Firmani, “Formation and structure of halos in a warm dark matter cosmology,” *Astrophys. J.* **559** (2001) 516–530, [arXiv:astro-ph/0010525 \[astro-ph\]](#).
- [57] P. Bode, J. P. Ostriker, and N. Turok, “Halo formation in warm dark matter models,” *Astrophys. J.* **556** (2001) 93–107, [arXiv:astro-ph/0010389 \[astro-ph\]](#).
- [58] A. Knebe, J. E. G. Devriendt, A. Mahmood, and J. Silk, “Merger histories in WDM structure formation scenarios,” *Mon. Not. Roy. Astron. Soc.* **329** (2002) 813, [arXiv:astro-ph/0105316 \[astro-ph\]](#).
- [59] M. R. Lovell, V. Eke, C. S. Frenk, L. Gao, A. Jenkins, T. Theuns, J. Wang, D. M. White, A. Boyarsky, and O. Ruchayskiy, “The Haloes of Bright Satellite Galaxies in a Warm Dark Matter Universe,” *Mon. Not. Roy. Astron. Soc.* **420** (2012) 2318–2324, [arXiv:1104.2929 \[astro-ph.CO\]](#).
- [60] A. Kamada, N. Yoshida, K. Kohri, and T. Takahashi, “Structure of Dark Matter Halos in Warm Dark Matter models and in models with Long-Lived Charged Massive Particles,” *JCAP* **1303** (2013) 008, [arXiv:1301.2744 \[astro-ph.CO\]](#).
- [61] W. Hu, R. Barkana, and A. Gruzinov, “Cold and fuzzy dark matter,” *Phys. Rev. Lett.* **85** (2000) 1158–1161, [arXiv:astro-ph/0003365 \[astro-ph\]](#).
- [62] T.-P. Woo and T. Chiueh, “High-Resolution Simulation on Structure Formation with Extremely Light Bosonic Dark Matter,” *Astrophys. J.* **697** (2009) 850–861, [arXiv:0806.0232 \[astro-ph\]](#).
- [63] D. J. E. Marsh and P. G. Ferreira, “Ultra-Light Scalar Fields and the Growth of Structure in the Universe,” *Phys. Rev.* **D82** (2010) 103528, [arXiv:1009.3501 \[hep-ph\]](#).

- [64] D. J. E. Marsh and J. Silk, “A Model For Halo Formation With Axion Mixed Dark Matter,” *Mon. Not. Roy. Astron. Soc.* **437** no. 3, (2014) 2652–2663, [arXiv:1307.1705 \[astro-ph.CO\]](#).
- [65] H.-Y. Schive, T. Chiueh, and T. Broadhurst, “Cosmic Structure as the Quantum Interference of a Coherent Dark Wave,” *Nature Phys.* **10** (2014) 496–499, [arXiv:1406.6586 \[astro-ph.GA\]](#).
- [66] H.-Y. Schive, M.-H. Liao, T.-P. Woo, S.-K. Wong, T. Chiueh, T. Broadhurst, and W. Y. P. Hwang, “Understanding the Core-Halo Relation of Quantum Wave Dark Matter from 3D Simulations,” *Phys. Rev. Lett.* **113** no. 26, (2014) 261302, [arXiv:1407.7762 \[astro-ph.GA\]](#).
- [67] D. J. E. Marsh and A.-R. Pop, “Axion dark matter, solitons and the cusp–core problem,” *Mon. Not. Roy. Astron. Soc.* **451** no. 3, (2015) 2479–2492, [arXiv:1502.03456 \[astro-ph.CO\]](#).
- [68] B. Schwabe, J. C. Niemeyer, and J. F. Engels, “Simulations of solitonic core mergers in ultralight axion dark matter cosmologies,” *Phys. Rev.* **D94** no. 4, (2016) 043513, [arXiv:1606.05151 \[astro-ph.CO\]](#).
- [69] L. Hui, J. P. Ostriker, S. Tremaine, and E. Witten, “Ultralight scalars as cosmological dark matter,” *Phys. Rev.* **D95** no. 4, (2017) 043541, [arXiv:1610.08297 \[astro-ph.CO\]](#).
- [70] J. Zhang, Y.-L. S. Tsai, J.-L. Kuo, K. Cheung, and M.-C. Chu, “Ultralight Axion Dark Matter and Its Impact on Dark Halo Structure in  $N$ -body Simulations,” *Astrophys. J.* **853** no. 1, (2018) 51, [arXiv:1611.00892 \[astro-ph.CO\]](#).
- [71] X. Du, B. Schwabe, J. C. Niemeyer, and D. Bürger, “Tidal disruption of fuzzy dark matter subhalo cores,” *Phys. Rev.* **D97** no. 6, (2018) 063507, [arXiv:1801.04864 \[astro-ph.GA\]](#).
- [72] C. Boehm, A. Riazuelo, S. H. Hansen, and R. Schaeffer, “Interacting dark matter disguised as warm dark matter,” *Phys. Rev.* **D66** (2002) 083505, [arXiv:astro-ph/0112522 \[astro-ph\]](#).
- [73] K. Sigurdson and M. Kamionkowski, “Charged - particle decay and suppression of small - scale power,” *Phys. Rev. Lett.* **92** (2004) 171302, [arXiv:astro-ph/0311486 \[astro-ph\]](#).
- [74] S. Profumo, K. Sigurdson, P. Ullio, and M. Kamionkowski, “A Running spectral index in supersymmetric dark-matter models with quasi-stable charged particles,” *Phys. Rev.* **D71** (2005) 023518, [arXiv:astro-ph/0410714 \[astro-ph\]](#).
- [75] L. G. van den Aarssen, T. Bringmann, and Y. C. Goedecke, “Thermal decoupling and the smallest subhalo mass in dark matter models with Sommerfeld-enhanced annihilation rates,” *Phys. Rev.* **D85** (2012) 123512, [arXiv:1202.5456 \[hep-ph\]](#).
- [76] L. G. van den Aarssen, T. Bringmann, and C. Pfrommer, “Is dark matter with long-range interactions a solution to all small-scale problems of  $\Lambda$  CDM cosmology?,” *Phys. Rev. Lett.* **109** (2012) 231301, [arXiv:1205.5809 \[astro-ph.CO\]](#).

- [77] C. Boehm, J. A. Schewtschenko, R. J. Wilkinson, C. M. Baugh, and S. Pascoli, “Using the Milky Way satellites to study interactions between cold dark matter and radiation,” *Mon. Not. Roy. Astron. Soc.* **445** (2014) L31–L35, [arXiv:1404.7012 \[astro-ph.CO\]](#).
- [78] M. R. Buckley, J. Zavala, F.-Y. Cyr-Racine, K. Sigurdson, and M. Vogelsberger, “Scattering, Damping, and Acoustic Oscillations: Simulating the Structure of Dark Matter Halos with Relativistic Force Carriers,” *Phys. Rev.* **D90** no. 4, (2014) 043524, [arXiv:1405.2075 \[astro-ph.CO\]](#).
- [79] J. A. Schewtschenko, R. J. Wilkinson, C. M. Baugh, C. Boehm, and S. Pascoli, “Dark matter–radiation interactions: the impact on dark matter haloes,” *Mon. Not. Roy. Astron. Soc.* **449** no. 4, (2015) 3587–3596, [arXiv:1412.4905 \[astro-ph.CO\]](#).
- [80] F.-Y. Cyr-Racine, K. Sigurdson, J. Zavala, T. Bringmann, M. Vogelsberger, and C. Pfrommer, “ETHOS—an effective theory of structure formation: From dark particle physics to the matter distribution of the Universe,” *Phys. Rev.* **D93** no. 12, (2016) 123527, [arXiv:1512.05344 \[astro-ph.CO\]](#).
- [81] M. Vogelsberger, J. Zavala, F.-Y. Cyr-Racine, C. Pfrommer, T. Bringmann, and K. Sigurdson, “ETHOS - An Effective Theory of Structure Formation: Dark matter physics as a possible explanation of the small-scale CDM problems,” *Mon. Not. Roy. Astron. Soc.* **460** (2016) 1399, [arXiv:1512.05349 \[astro-ph.CO\]](#).
- [82] J. A. Schewtschenko, C. M. Baugh, R. J. Wilkinson, C. Boehm, S. Pascoli, and T. Sawala, “Dark matter–radiation interactions: the structure of Milky Way satellite galaxies,” *Mon. Not. Roy. Astron. Soc.* **461** no. 3, (2016) 2282–2287, [arXiv:1512.06774 \[astro-ph.CO\]](#).
- [83] T. Binder, L. Covi, A. Kamada, H. Murayama, T. Takahashi, and N. Yoshida, “Matter Power Spectrum in Hidden Neutrino Interacting Dark Matter Models: A Closer Look at the Collision Term,” *JCAP* **1611** (2016) 043, [arXiv:1602.07624 \[hep-ph\]](#).
- [84] T. Bringmann, H. T. Ihle, J. Kersten, and P. Walia, “Suppressing structure formation at dwarf galaxy scales and below: late kinetic decoupling as a compelling alternative to warm dark matter,” *Phys. Rev.* **D94** no. 10, (2016) 103529, [arXiv:1603.04884 \[hep-ph\]](#).
- [85] A. Kamada and T. Takahashi, “Dark matter kinetic decoupling with a light particle,” *JCAP* **1801** no. 01, (2018) 047, [arXiv:1703.02338 \[astro-ph.CO\]](#).
- [86] T. Moroi, H. Murayama, and M. Yamaguchi, “Cosmological constraints on the light stable gravitino,” *Phys. Lett.* **B303** (1993) 289–294.
- [87] E. Pierpaoli, S. Borgani, A. Masiero, and M. Yamaguchi, “The Formation of cosmic structures in a light gravitino dominated universe,” *Phys. Rev.* **D57** (1998) 2089–2100, [arXiv:astro-ph/9709047 \[astro-ph\]](#).
- [88] R. Murgia, A. Merle, M. Viel, M. Totzauer, and A. Schneider, ““Non-cold” dark matter at small scales: a general approach,” *JCAP* **1711** (2017) 046, [arXiv:1704.07838 \[astro-ph.CO\]](#).
- [89] R. Murgia, V. Iri, and M. Viel, “Novel constraints on noncold, nonthermal dark matter from Lyman- forest data,” *Phys. Rev.* **D98** no. 8, (2018) 083540, [arXiv:1806.08371 \[astro-ph.CO\]](#).

- [90] L. J. Hall, K. Jedamzik, J. March-Russell, and S. M. West, “Freeze-In Production of FIMP Dark Matter,” *JHEP* **03** (2010) 080, [arXiv:0911.1120 \[hep-ph\]](#).
- [91] N. Bernal, M. Heikinheimo, T. Tenkanen, K. Tuominen, and V. Vaskonen, “The Dawn of FIMP Dark Matter: A Review of Models and Constraints,” *Int. J. Mod. Phys. A* **32** no. 27, (2017) 1730023, [arXiv:1706.07442 \[hep-ph\]](#).
- [92] M. Shaposhnikov and I. Tkachev, “The nuMSM, inflation, and dark matter,” *Phys. Lett.* **B639** (2006) 414–417, [arXiv:hep-ph/0604236 \[hep-ph\]](#).
- [93] D. Gorbunov, A. Khmelnitsky, and V. Rubakov, “Is gravitino still a warm dark matter candidate?,” *JHEP* **12** (2008) 055, [arXiv:0805.2836 \[hep-ph\]](#).
- [94] D. Boyanovsky, “Clustering properties of a sterile neutrino dark matter candidate,” *Phys. Rev.* **D78** (2008) 103505, [arXiv:0807.0646 \[astro-ph\]](#).
- [95] A. Adulpravitchai and M. A. Schmidt, “Sterile Neutrino Dark Matter Production in the Neutrino-phillic Two Higgs Doublet Model,” *JHEP* **12** (2015) 023, [arXiv:1507.05694 \[hep-ph\]](#).
- [96] J. McDonald, “Warm Dark Matter via Ultra-Violet Freeze-In: Reheating Temperature and Non-Thermal Distribution for Fermionic Higgs Portal Dark Matter,” *JCAP* **1608** no. 08, (2016) 035, [arXiv:1512.06422 \[hep-ph\]](#).
- [97] S. B. Roland and B. Shakya, “Cosmological Imprints of Frozen-In Light Sterile Neutrinos,” *JCAP* **1705** no. 05, (2017) 027, [arXiv:1609.06739 \[hep-ph\]](#).
- [98] J. Heeck and D. Teresi, “Cold keV dark matter from decays and scatterings,” *Phys. Rev.* **D96** no. 3, (2017) 035018, [arXiv:1706.09909 \[hep-ph\]](#).
- [99] K. J. Bae, A. Kamada, S. P. Liew, and K. Yanagi, “Light axinos from freeze-in: production processes, phase space distributions, and Ly- $\alpha$  forest constraints,” *JCAP* **1801** no. 01, (2018) 054, [arXiv:1707.06418 \[hep-ph\]](#).
- [100] S. Dodelson and L. M. Widrow, “Sterile-neutrinos as dark matter,” *Phys. Rev. Lett.* **72** (1994) 17–20, [arXiv:hep-ph/9303287 \[hep-ph\]](#).
- [101] S. Colombi, S. Dodelson, and L. M. Widrow, “Large scale structure tests of warm dark matter,” *Astrophys. J.* **458** (1996) 1, [arXiv:astro-ph/9505029 \[astro-ph\]](#).
- [102] K. Abazajian, “Production and evolution of perturbations of sterile neutrino dark matter,” *Phys. Rev.* **D73** (2006) 063506, [arXiv:astro-ph/0511630 \[astro-ph\]](#).
- [103] T. Venumadhav, F.-Y. Cyr-Racine, K. N. Abazajian, and C. M. Hirata, “Sterile neutrino dark matter: Weak interactions in the strong coupling epoch,” *Phys. Rev.* **D94** no. 4, (2016) 043515, [arXiv:1507.06655 \[astro-ph.CO\]](#).
- [104] M. Kaplinghat, “Dark matter from early decays,” *Phys. Rev.* **D72** (2005) 063510, [arXiv:astro-ph/0507300 \[astro-ph\]](#).
- [105] K. Petraki and A. Kusenko, “Dark-matter sterile neutrinos in models with a gauge singlet in the Higgs sector,” *Phys. Rev.* **D77** (2008) 065014, [arXiv:0711.4646 \[hep-ph\]](#).

- [106] A. Merle and A. Schneider, “Production of Sterile Neutrino Dark Matter and the 3.5 keV line,” *Phys. Lett.* **B749** (2015) 283–288, [arXiv:1409.6311 \[hep-ph\]](#).
- [107] F. Bezrukov and D. Gorbunov, “Applicability of approximations used in calculations of the spectrum of dark matter particles produced in particle decays,” *Phys. Rev.* **D93** no. 6, (2016) 063502, [arXiv:1412.1341 \[hep-ph\]](#).
- [108] A. Merle and M. Totzauer, “keV Sterile Neutrino Dark Matter from Singlet Scalar Decays: Basic Concepts and Subtle Features,” *JCAP* **1506** (2015) 011, [arXiv:1502.01011 \[hep-ph\]](#).
- [109] J. König, A. Merle, and M. Totzauer, “keV Sterile Neutrino Dark Matter from Singlet Scalar Decays: The Most General Case,” *JCAP* **1611** no. 11, (2016) 038, [arXiv:1609.01289 \[hep-ph\]](#).
- [110] D. Blas, J. Lesgourgues, and T. Tram, “The Cosmic Linear Anisotropy Solving System (CLASS) II: Approximation schemes,” *JCAP* **1107** (2011) 034, [arXiv:1104.2933 \[astro-ph.CO\]](#).
- [111] J. Lesgourgues and T. Tram, “The Cosmic Linear Anisotropy Solving System (CLASS) IV: efficient implementation of non-cold relics,” *JCAP* **1109** (2011) 032, [arXiv:1104.2935 \[astro-ph.CO\]](#).
- [112] **Planck** Collaboration, P. A. R. Ade *et al.*, “Planck 2015 results. XIII. Cosmological parameters,” *Astron. Astrophys.* **594** (2016) A13, [arXiv:1502.01589 \[astro-ph.CO\]](#).
- [113] A. V. Maccio and F. Fontanot, “How cold is Dark Matter? Constraints from Milky Way Satellites,” *Mon. Not. Roy. Astron. Soc.* **404** (2010) 16, [arXiv:0910.2460 \[astro-ph.CO\]](#).
- [114] E. Polisensky and M. Ricotti, “Constraints on the Dark Matter Particle Mass from the Number of Milky Way Satellites,” *Phys. Rev.* **D83** (2011) 043506, [arXiv:1004.1459 \[astro-ph.CO\]](#).
- [115] M. R. Lovell, C. S. Frenk, V. R. Eke, A. Jenkins, L. Gao, and T. Theuns, “The properties of warm dark matter haloes,” *Mon. Not. Roy. Astron. Soc.* **439** (2014) 300–317, [arXiv:1308.1399 \[astro-ph.CO\]](#).
- [116] R. Kennedy, C. Frenk, S. Cole, and A. Benson, “Constraining the warm dark matter particle mass with Milky Way satellites,” *Mon. Not. Roy. Astron. Soc.* **442** no. 3, (2014) 2487–2495, [arXiv:1310.7739 \[astro-ph.CO\]](#).
- [117] S. Horiuchi, P. J. Humphrey, J. Onorbe, K. N. Abazajian, M. Kaplinghat, and S. Garrison-Kimmel, “Sterile neutrino dark matter bounds from galaxies of the Local Group,” *Phys. Rev.* **D89** no. 2, (2014) 025017, [arXiv:1311.0282 \[astro-ph.CO\]](#).
- [118] A. Schneider, “Structure formation with suppressed small-scale perturbations,” *Mon. Not. Roy. Astron. Soc.* **451** no. 3, (2015) 3117–3130, [arXiv:1412.2133 \[astro-ph.CO\]](#).
- [119] M. Viel, J. Lesgourgues, M. G. Haehnelt, S. Matarrese, and A. Riotto, “Constraining warm dark matter candidates including sterile neutrinos and light gravitinos with WMAP and the Lyman-alpha forest,” *Phys. Rev.* **D71** (2005) 063534, [arXiv:astro-ph/0501562 \[astro-ph\]](#).

- [120] U. Seljak, A. Makarov, P. McDonald, and H. Trac, “Can sterile neutrinos be the dark matter?,” *Phys. Rev. Lett.* **97** (2006) 191303, [arXiv:astro-ph/0602430](#) [[astro-ph](#)].
- [121] M. Viel, J. Lesgourgues, M. G. Haehnelt, S. Matarrese, and A. Riotto, “Can sterile neutrinos be ruled out as warm dark matter candidates?,” *Phys. Rev. Lett.* **97** (2006) 071301, [arXiv:astro-ph/0605706](#) [[astro-ph](#)].
- [122] M. Viel, G. D. Becker, J. S. Bolton, M. G. Haehnelt, M. Rauch, and W. L. W. Sargent, “How cold is cold dark matter? Small scales constraints from the flux power spectrum of the high-redshift Lyman-alpha forest,” *Phys. Rev. Lett.* **100** (2008) 041304, [arXiv:0709.0131](#) [[astro-ph](#)].
- [123] M. Viel, G. D. Becker, J. S. Bolton, and M. G. Haehnelt, “Warm dark matter as a solution to the small scale crisis: New constraints from high redshift Lyman- $\alpha$  forest data,” *Phys. Rev.* **D88** (2013) 043502, [arXiv:1306.2314](#) [[astro-ph.CO](#)].
- [124] J. Baur, N. Palanque-Delabrouille, C. Yèche, C. Magneville, and M. Viel, “Lyman-alpha Forests cool Warm Dark Matter,” *JCAP* **1608** no. 08, (2016) 012, [arXiv:1512.01981](#) [[astro-ph.CO](#)].
- [125] C. Yèche, N. Palanque-Delabrouille, J. Baur, and H. du Mas des Bourboux, “Constraints on neutrino masses from Lyman-alpha forest power spectrum with BOSS and XQ-100,” [arXiv:1702.03314](#) [[astro-ph.CO](#)].
- [126] V. Iršič *et al.*, “New Constraints on the free-streaming of warm dark matter from intermediate and small scale Lyman- $\alpha$  forest data,” [arXiv:1702.01764](#) [[astro-ph.CO](#)].
- [127] E. Armengaud, N. Palanque-Delabrouille, C. Yèche, D. J. E. Marsh, and J. Baur, “Constraining the mass of light bosonic dark matter using SDSS Lyman- $\alpha$  forest,” *Mon. Not. Roy. Astron. Soc.* **471** no. 4, (2017) 4606–4614, [arXiv:1703.09126](#) [[astro-ph.CO](#)].
- [128] T. Kobayashi, R. Murgia, A. De Simone, V. Iršič, and M. Viel, “Lyman- $\alpha$  constraints on ultralight scalar dark matter: Implications for the early and late universe,” *Phys. Rev.* **D96** no. 12, (2017) 123514, [arXiv:1708.00015](#) [[astro-ph.CO](#)].
- [129] J. Zhang, J.-L. Kuo, H. Liu, Y.-L. S. Tsai, K. Cheung, and M.-C. Chu, “The Importance of Quantum Pressure of Fuzzy Dark Matter on Lyman-Alpha Forest,” *Astrophys. J.* **863** (2018) 73, [arXiv:1708.04389](#) [[astro-ph.CO](#)].
- [130] M. Nori, R. Murgia, V. Iršič, M. Baldi, and M. Viel, “Lyman  $\alpha$  forest and non-linear structure characterization in Fuzzy Dark Matter cosmologies,” *Mon. Not. Roy. Astron. Soc.* **482** no. 3, (2019) 3227–3243, [arXiv:1809.09619](#) [[astro-ph.CO](#)].
- [131] K.-H. Leong, H.-Y. Schive, U.-H. Zhang, and T. Chiueh, “Testing extreme-axion wave-like dark matter using the BOSS Lyman-alpha forest data,” *Mon. Not. Roy. Astron. Soc.* **484** no. 3, (2019) 4273–4286, [arXiv:1810.05930](#) [[astro-ph.CO](#)].
- [132] S. Bose, M. Vogelsberger, J. Zavala, C. Pfrommer, F.-Y. Cyr-Racine, S. Bohr, and T. Bringmann, “ETHOS - an Effective Theory of Structure Formation: detecting dark matter interactions through the Lyman- $\alpha$  forest,” [arXiv:1811.10630](#) [[astro-ph.CO](#)].

- [133] R. Barkana, Z. Haiman, and J. P. Ostriker, “Constraints on warm dark matter from cosmological reionization,” *Astrophys. J.* **558** (2001) 482, [arXiv:astro-ph/0102304](#) [[astro-ph](#)].
- [134] N. Yoshida, A. Sokasian, L. Hernquist, and V. Springel, “Early structure formation and reionization in a warm dark matter cosmology,” *Astrophys. J.* **591** (2003) L1–L4, [arXiv:astro-ph/0303622](#) [[astro-ph](#)].
- [135] C. Schultz, J. Oñorbe, K. N. Abazajian, and J. S. Bullock, “The High- $z$  Universe Confronts Warm Dark Matter: Galaxy Counts, Reionization and the Nature of Dark Matter,” *Mon. Not. Roy. Astron. Soc.* **442** no. 2, (2014) 1597–1609, [arXiv:1401.3769](#) [[astro-ph.CO](#)].
- [136] A. Lapi and L. Danese, “Cold or Warm? Constraining Dark Matter with Primeval Galaxies and Cosmic Reionization after Planck,” *JCAP* **1509** no. 09, (2015) 003, [arXiv:1508.02147](#) [[astro-ph.CO](#)].
- [137] W.-W. Tan, F. Y. Wang, and K. S. Cheng, “Constraining warm dark matter mass with cosmic reionization and gravitational wave,” *Astrophys. J.* **829** no. 1, (2016) 29, [arXiv:1607.03567](#) [[astro-ph.CO](#)].
- [138] L. Lopez-Honorez, O. Mena, S. Palomares-Ruiz, and P. Villanueva-Domingo, “Warm dark matter and the ionization history of the Universe,” *Phys. Rev.* **D96** no. 10, (2017) 103539, [arXiv:1703.02302](#) [[astro-ph.CO](#)].
- [139] M. R. Lovell, J. Zavala, M. Vogelsberger, X. Shen, F.-Y. Cyr-Racine, C. Pfrommer, K. Sigurdson, M. Boylan-Kolchin, and A. Pillepich, “ETHOS – an effective theory of structure formation: predictions for the high-redshift Universe – abundance of galaxies and reionization,” *Mon. Not. Roy. Astron. Soc.* **477** no. 3, (2018) 2886–2899, [arXiv:1711.10497](#) [[astro-ph.CO](#)].
- [140] A. Mesinger, R. Perna, and Z. Haiman, “Constraints on the small-scale power spectrum of density fluctuations from high-redshift gamma-ray bursts,” *Astrophys. J.* **623** (2005) 1–10, [arXiv:astro-ph/0501233](#) [[astro-ph](#)].
- [141] R. S. de Souza, A. Mesinger, A. Ferrara, Z. Haiman, R. Perna, and N. Yoshida, “Constraints on Warm Dark Matter models from high-redshift long gamma-ray bursts,” *Mon. Not. Roy. Astron. Soc.* **432** (2013) 3218, [arXiv:1303.5060](#) [[astro-ph.CO](#)].
- [142] F. Pacucci, A. Mesinger, and Z. Haiman, “Focusing on Warm Dark Matter with Lensed High-redshift Galaxies,” *Mon. Not. Roy. Astron. Soc.* **435** (2013) L53, [arXiv:1306.0009](#) [[astro-ph.CO](#)].
- [143] H.-Y. Schive, T. Chiueh, T. Broadhurst, and K.-W. Huang, “Contrasting Galaxy Formation from Quantum Wave Dark Matter,  $\psi$ DM, with  $\Lambda$ CDM, using Planck and Hubble Data,” *Astrophys. J.* **818** no. 1, (2016) 89, [arXiv:1508.04621](#) [[astro-ph.GA](#)].
- [144] N. Menci, N. G. Sanchez, M. Castellano, and A. Grazian, “Constraining the Warm Dark Matter Particle Mass through Ultra-Deep UV Luminosity Functions at  $z = 2$ ,” *Astrophys. J.* **818** no. 1, (2016) 90, [arXiv:1601.01820](#) [[astro-ph.CO](#)].

- [145] N. Menci, A. Grazian, M. Castellano, and N. G. Sanchez, “A Stringent Limit on the Warm Dark Matter Particle Masses from the Abundance of  $z=6$  Galaxies in the Hubble Frontier Fields,” *Astrophys. J.* **825** no. 1, (2016) L1, [arXiv:1606.02530 \[astro-ph.CO\]](#).
- [146] Y. Ni, M.-Y. Wang, Y. Feng, and T. Di Matteo, “Predictions for the Abundance of High-redshift Galaxies in a Fuzzy Dark Matter Universe,” [arXiv:1904.01604 \[astro-ph.CO\]](#).
- [147] M. Miranda and A. V. Maccio, “Constraining Warm Dark Matter using QSO gravitational lensing,” *Mon. Not. Roy. Astron. Soc.* **382** (2007) 1225, [arXiv:0706.0896 \[astro-ph\]](#).
- [148] K. T. Inoue, R. Takahashi, T. Takahashi, and T. Ishiyama, “Constraints on warm dark matter from weak lensing in anomalous quadruple lenses,” *Mon. Not. Roy. Astron. Soc.* **448** no. 3, (2015) 2704–2716, [arXiv:1409.1326 \[astro-ph.CO\]](#).
- [149] A. Kamada, K. T. Inoue, and T. Takahashi, “Constraints on mixed dark matter from anomalous strong lens systems,” *Phys. Rev.* **D94** no. 2, (2016) 023522, [arXiv:1604.01489 \[astro-ph.CO\]](#).
- [150] A. Kamada, K. T. Inoue, K. Kohri, and T. Takahashi, “Constraints on long-lived electrically charged massive particles from anomalous strong lens systems,” *JCAP* **1711** no. 11, (2017) 008, [arXiv:1703.05145 \[astro-ph.CO\]](#).
- [151] S. Birrer, A. Amara, and A. Refregier, “Lensing substructure quantification in RXJ1131-1231: A 2 keV lower bound on dark matter thermal relic mass,” *JCAP* **1705** no. 05, (2017) 037, [arXiv:1702.00009 \[astro-ph.CO\]](#).
- [152] D. Gilman, S. Birrer, T. Treu, C. R. Keeton, and A. Nierenberg, “Probing the nature of dark matter by forward modelling flux ratios in strong gravitational lenses,” *Mon. Not. Roy. Astron. Soc.* **481** no. 1, (2018) 819–834, [arXiv:1712.04945 \[astro-ph.CO\]](#).
- [153] S. Vegetti, G. Despali, M. R. Lovell, and W. Enzi, “Constraining sterile neutrino cosmologies with strong gravitational lensing observations at redshift  $z \sim 0.2$ ,” *Mon. Not. Roy. Astron. Soc.* **481** no. 3, (2018) 3661–3669, [arXiv:1801.01505 \[astro-ph.CO\]](#).
- [154] A. Díaz Rivero, C. Dvorkin, F.-Y. Cyr-Racine, J. Zavala, and M. Vogelsberger, “Gravitational Lensing and the Power Spectrum of Dark Matter Substructure: Insights from the ETHOS N-body Simulations,” *Phys. Rev.* **D98** no. 10, (2018) 103517, [arXiv:1809.00004 \[astro-ph.CO\]](#).
- [155] M. Sitwell, A. Mesinger, Y.-Z. Ma, and K. Sigurdson, “The Imprint of Warm Dark Matter on the Cosmological 21-cm Signal,” *Mon. Not. Roy. Astron. Soc.* **438** no. 3, (2014) 2664–2671, [arXiv:1310.0029 \[astro-ph.CO\]](#).
- [156] T. Sekiguchi and H. Tashiro, “Constraining warm dark matter with 21 cm line fluctuations due to minihalos,” *JCAP* **1408** (2014) 007, [arXiv:1401.5563 \[astro-ph.CO\]](#).
- [157] M. Safarzadeh, E. Scannapieco, and A. Babul, “A limit on the warm dark matter particle mass from the redshifted 21 cm absorption line,” *Astrophys. J.* **859** no. 2, (2018) L18, [arXiv:1803.08039 \[astro-ph.CO\]](#).



- [158] A. Schneider, “Constraining noncold dark matter models with the global 21-cm signal,” *Phys. Rev.* **D98** no. 6, (2018) 063021, [arXiv:1805.00021 \[astro-ph.CO\]](#).
- [159] A. Lidz and L. Hui, “Implications of a preionization 21-cm absorption signal for fuzzy dark matter,” *Phys. Rev.* **D98** no. 2, (2018) 023011, [arXiv:1805.01253 \[astro-ph.CO\]](#).
- [160] L. Lopez-Honorez, O. Mena, and P. Villanueva-Domingo, “Dark matter microphysics and 21 cm observations,” *Phys. Rev.* **D99** no. 2, (2019) 023522, [arXiv:1811.02716 \[astro-ph.CO\]](#).
- [161] O. Nebrin, R. Ghara, and G. Mellema, “Fuzzy Dark Matter at Cosmic Dawn: New 21-cm Constraints,” *JCAP* **1904** no. 04, (2019) 051, [arXiv:1812.09760 \[astro-ph.CO\]](#).
- [162] A. Chatterjee, P. Dayal, T. R. Choudhury, and A. Hutter, “Ruling out 3 keV warm dark matter using 21 cm-EDGES data,” [arXiv:1902.09562 \[astro-ph.CO\]](#).
- [163] S. Pandolfi, C. Evoli, A. Ferrara, and F. Villaescusa-Navarro, “Constraining Warm Dark Matter with high- $z$  supernova lensing,” *Mon. Not. Roy. Astron. Soc.* **442** no. 1, (2014) 13–19, [arXiv:1403.2185 \[astro-ph.CO\]](#).
- [164] P. Dayal, T. R. Choudhury, F. Pacucci, and V. Bromm, “Warm dark matter constraints from high- $z$  Direct Collapse Black Holes using the JWST,” *Mon. Not. Roy. Astron. Soc.* **472** no. 4, (2017) 4414–4421, [arXiv:1705.00632 \[astro-ph.CO\]](#).
- [165] F. Governato, L. Mayer, J. Wadsley, J. P. Gardner, B. Willman, E. Hayashi, T. R. Quinn, J. Stadel, and G. Lake, “The Formation of a realistic disk galaxy in lambda dominated cosmologies,” *Astrophys. J.* **607** (2004) 688–696, [arXiv:astro-ph/0207044 \[astro-ph\]](#).
- [166] L. Gao and T. Theuns, “Lighting the Universe with filaments,” *Science* **317** (2007) 1527, [arXiv:0709.2165 \[astro-ph\]](#).
- [167] J. Herpich, G. S. Stinson, A. V. Macciò, C. Brook, J. Wadsley, H. M. P. Couchman, and T. Quinn, “MaGICC-WDM: the effects of warm dark matter in hydrodynamical simulations of disc galaxy formation,” *Mon. Not. Roy. Astron. Soc.* **437** no. 1, (2014) 293–304, [arXiv:1308.1088 \[astro-ph.CO\]](#).
- [168] F. Governato *et al.*, “Faint dwarfs as a test of DM models: WDM versus CDM,” *Mon. Not. Roy. Astron. Soc.* **448** no. 1, (2015) 792–803, [arXiv:1407.0022 \[astro-ph.GA\]](#).
- [169] U. Maio and M. Viel, “The First Billion Years of a Warm Dark Matter Universe,” *Mon. Not. Roy. Astron. Soc.* **446** (2015) 2760–2775, [arXiv:1409.6718 \[astro-ph.CO\]](#).
- [170] P. Colin, V. Avila-Reese, A. Gonzalez-Samaniego, and H. Velazquez, “Simulations of galaxies formed in warm dark matter halos of masses at the filtering scale,” *Astrophys. J.* **803** no. 1, (2015) 28, [arXiv:1412.1100 \[astro-ph.GA\]](#).
- [171] A. Gonzalez-Samaniego, V. Avila-Reese, and P. Colin, “The inner structure of dwarf sized halos in Warm and Cold Dark Matter cosmologies,” *Astrophys. J.* **819** (2016) 101, [arXiv:1512.03538 \[astro-ph.GA\]](#).
- [172] M. R. Lovell *et al.*, “Properties of Local Group galaxies in hydrodynamical simulations of sterile neutrino dark matter cosmologies,” *Mon. Not. Roy. Astron. Soc.* **468** no. 4, (2017) 4285–4298, [arXiv:1611.00010 \[astro-ph.GA\]](#).

- [173] L. Wang, V. Gonzalez-Perez, L. Xie, A. P. Cooper, C. S. Frenk, L. Gao, W. A. Hellwing, J. Helly, M. R. Lovell, and L. Jiang, “The galaxy population in cold and warm dark matter cosmologies,” *Mon. Not. Roy. Astron. Soc.* **468** no. 4, (2017) 4579–4591, [arXiv:1612.04540 \[astro-ph.GA\]](#).
- [174] P. Villanueva-Domingo, N. Y. Gnedin, and O. Mena, “Warm Dark Matter and Cosmic Reionization,” *Astrophys. J.* **852** no. 2, (2018) 139, [arXiv:1708.08277 \[astro-ph.CO\]](#).
- [175] B. Bozek *et al.*, “Warm FIRE: Simulating Galaxy Formation with Resonant Sterile Neutrino Dark Matter,” [arXiv:1803.05424 \[astro-ph.GA\]](#).
- [176] J. Bremer, P. Dayal, and E. V. Ryan-Weber, “Probing the nature of Dark Matter through the metal enrichment of the intergalactic medium,” *Mon. Not. Roy. Astron. Soc.* **477** no. 2, (2018) 2154–2163, [arXiv:1803.05450 \[astro-ph.GA\]](#).
- [177] A. Fitts *et al.*, “Dwarf Galaxies in CDM, WDM, and SIDM: Disentangling Baryons and Dark Matter Physics,” [arXiv:1811.11791 \[astro-ph.GA\]](#).
- [178] M. R. Lovell, J. Zavala, and M. Vogelsberger, “ETHOS - an effective theory of structure formation: formation of the first haloes and their stars,” *Mon. Not. Roy. Astron. Soc.* **485** no. 4, (2019) 5474–5489, [arXiv:1812.04627 \[astro-ph.GA\]](#).
- [179] A. V. Macciò, J. Frings, T. Buck, A. A. Dutton, M. Blank, A. Obreja, and K. L. Dixon, “The edge of galaxy formation III: The effects of warm dark matter on Milky Way satellites and field dwarfs,” [arXiv:1902.02047 \[astro-ph.GA\]](#).
- [180] A. Schneider, “Astrophysical constraints on resonantly produced sterile neutrino dark matter,” *JCAP* **1604** no. 04, (2016) 059, [arXiv:1601.07553 \[astro-ph.CO\]](#).
- [181] C. G. Lacey and S. Cole, “Merger rates in hierarchical models of galaxy formation,” *Mon. Not. Roy. Astron. Soc.* **262** (1993) 627–649.
- [182] W. H. Press and P. Schechter, “Formation of galaxies and clusters of galaxies by selfsimilar gravitational condensation,” *Astrophys. J.* **187** (1974) 425–438.
- [183] A. Cooray and R. K. Sheth, “Halo Models of Large Scale Structure,” *Phys. Rept.* **372** (2002) 1–129, [arXiv:astro-ph/0206508 \[astro-ph\]](#).
- [184] V. Springel, J. Wang, M. Vogelsberger, A. Ludlow, A. Jenkins, A. Helmi, J. F. Navarro, C. S. Frenk, and S. D. M. White, “The Aquarius Project: the subhalos of galactic halos,” *Mon. Not. Roy. Astron. Soc.* **391** (2008) 1685–1711, [arXiv:0809.0898 \[astro-ph\]](#).
- [185] M. G. Walker, M. Mateo, E. W. Olszewski, J. Penarrubia, N. W. Evans, and G. Gilmore, “A Universal Mass Profile for Dwarf Spheroidal Galaxies,” *Astrophys. J.* **704** (2009) 1274–1287, [arXiv:0906.0341 \[astro-ph.CO\]](#). [Erratum: *Astrophys. J.* 710,886(2010)].
- [186] J. Wolf, G. D. Martinez, J. S. Bullock, M. Kaplinghat, M. Geha, R. R. Munoz, J. D. Simon, and F. F. Avedo, “Accurate Masses for Dispersion-supported Galaxies,” *Mon. Not. Roy. Astron. Soc.* **406** (2010) 1220, [arXiv:0908.2995 \[astro-ph.CO\]](#).
- [187] A. Schneider, D. Anderhalden, A. Maccio, and J. Diemand, “Warm dark matter does not do better than cold dark matter in solving small-scale inconsistencies,” *Mon. Not. Roy. Astron. Soc.* **441** (2014) 6, [arXiv:1309.5960 \[astro-ph.CO\]](#).

- [188] S. H. Hansen, J. Lesgourgues, S. Pastor, and J. Silk, “Constraining the window on sterile neutrinos as warm dark matter,” *Mon. Not. Roy. Astron. Soc.* **333** (2002) 544–546, [arXiv:astro-ph/0106108 \[astro-ph\]](#).
- [189] K. J. Bae, A. Kamada, S. P. Liew, and K. Yanagi, “Colder Freeze-in Axinos Decaying into Photons,” *Phys. Rev.* **D97** no. 5, (2018) 055019, [arXiv:1707.02077 \[hep-ph\]](#).
- [190] A. R. Zhitnitsky, “On Possible Suppression of the Axion Hadron Interactions. (In Russian),” *Sov. J. Nucl. Phys.* **31** (1980) 260. [*Yad. Fiz.*31,497(1980)].
- [191] M. Dine, W. Fischler, and M. Srednicki, “A Simple Solution to the Strong CP Problem with a Harmless Axion,” *Phys. Lett.* **B104** (1981) 199–202.
- [192] R. D. Peccei and H. R. Quinn, “CP Conservation in the Presence of Instantons,” *Phys. Rev. Lett.* **38** (1977) 1440–1443.
- [193] R. D. Peccei and H. R. Quinn, “Constraints Imposed by CP Conservation in the Presence of Instantons,” *Phys. Rev.* **D16** (1977) 1791–1797.
- [194] S. Weinberg, “A New Light Boson?,” *Phys. Rev. Lett.* **40** (1978) 223–226.
- [195] F. Wilczek, “Problem of Strong p and t Invariance in the Presence of Instantons,” *Phys. Rev. Lett.* **40** (1978) 279–282.
- [196] R. Jinno, “Machine learning for bounce calculation,” [arXiv:1805.12153 \[hep-th\]](#).
- [197] V. Nair and G. E. Hinton, “Rectified linear units improve restricted boltzmann machines,” in *Proceedings of the 27th International Conference on International Conference on Machine Learning, ICML’10*, pp. 807–814. Omnipress, USA, 2010. <http://dl.acm.org/citation.cfm?id=3104322.3104425>.
- [198] “Tensorflow.” <https://www.tensorflow.org/>.
- [199] N. Srivastava, G. Hinton, A. Krizhevsky, I. Sutskever, and R. Salakhutdinov, “Dropout: A simple way to prevent neural networks from overfitting,” *J. Mach. Learn. Res.* **15** no. 1, (Jan., 2014) 1929–1958. <http://dl.acm.org/citation.cfm?id=2627435.2670313>.
- [200] D. P. Kingma and J. Ba, “Adam: A Method for Stochastic Optimization,” [arXiv:1412.6980 \[cs.LG\]](#).
- [201] J. R. Bond, A. S. Szalay, and M. S. Turner, “Formation of Galaxies in a Gravitino Dominated Universe,” *Phys. Rev. Lett.* **48** (1982) 1636.
- [202] J. R. Bond and A. S. Szalay, “The Collisionless Damping of Density Fluctuations in an Expanding Universe,” *Astrophys. J.* **274** (1983) 443–468.
- [203] J. R. Bond, G. Efstathiou, and J. Silk, “Massive Neutrinos and the Large Scale Structure of the Universe,” *Phys. Rev. Lett.* **45** (1980) 1980–1984. [*61*(1980)].
- [204] M. Davis, M. Lecar, C. Pryor, and E. Witten, “The Formation of Galaxies From Massive Neutrinos,” *Astrophys. J.* **250** (1981) 423–431.

- [205] P. J. E. Peebles, “PRIMEVAL ADIABATIC PERTURBATIONS: EFFECT OF MASSIVE NEUTRINOS,” *Astrophys. J.* **258** (1982) 415–424.
- [206] A. Kamada and K. Yanagi. in preparation.